FINAL TECHNICAL REPORT

TO

THE OFFICE OF NAVAL RESEARCH

800 NORTH QUINCY STREET

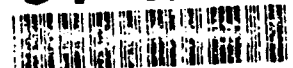ARLINGTON, VIRGINIA 22217-5000

Attention: Joseph Kravitz

for

ACOUSTICAL AND OTHER PHYSICAL PROPERTIES OF MARINE

SEDIMENTS

GRANT NO: N00014-89-J-1316 MOD/AMEND: P00002

Investigator: Amos Nur

91-17273

ONR CONTRACT N00014-89-J-1316-P03: THE SUMMARY OF THE RESEARCH ACCOMPLISHED

The results of the research effort include four parts:

1. a) The Effect of Cementation on the Elastic Properties of Granular Material and b) Seismic Velocities in Compacting Sediments

2. a) The Mechanics of Hollow Grains and b) Pillow Basalts Compaction due to Grain Collapse

3. Modeling the Granular Structure of Rocks

4. Anisotropic Poroelasticity and Biot's Parameters

PART 1 A simple analytical model has been developed to describe the mechanics of cemented granular material, for which a solution has been obtained to model the normal and shear deformation of a cement layer with straight boundaries. The problem of the normal compression of two contacting circular elastic grains and an elastic cement layer between them has been reduced to a linear integral equation. This problem has been solved both for two-dimensional (cylindrical grains) and three-dimensional (spherical grains) cases. The elastic modulus of such a combination is strongly increased by cementation compared to the case of a classic Hertzian contact. The stiffness of the cemented system increases with the length of the cement layer and with the relative stiffness of the cement. It significantly exceeds the stiffness of the Hertzian system at low confining pressure. A small increase in the amount of cementation results in significant growth of the contact zone between grains and, thus, dramatically increases the stiffness of the system.

The theory of cementation is used in a theoretical model for the compaction

1

of sediments formed by quartz grains separated at their contacts by a cementing component. Compaction occurs due to lithostatic pressure that results in increasing contact stresses with burial. As the stresses at the contacts become larger, the cementing material yields, the separation between the grains decreases, and the radius of the contact becomes larger. This changing geometry gives rise to an increase of P- and S- velocity with confining pressure, and therefore with depth. Seismic velocities are evaluated using standard formulas relating the elastic properties of granular material to the contact stiffness between two grains and the average number of contacts per grain. Velocities increase rapidly during the initial stage of compaction. As compaction continues, the velocities gradually approach constant values that correspond to direct contact of the grains. An interesting effect of smooth peaks in P- and S-velocity before they reach their constant values is predicted if cementation is very soft compared to the grain material (e.g. quartz grains in silt). This is due to the fact that the normal stiffness of two spherical grains separated by a thin layer of a soft cement can be higher than that of directly contacting grains.

PART 2 In order to model the mechanical behavior of pillow basalts, we have developed a theory for the two-dimensional deformation of hollow grains under external loading. We model the grains as cylindrical shells of a closed cross-section. This theory allows us to describe the deformation of arbitrarily-shaped grains with walls of varying thickness. Calculating the normal and shear stiffness of hollow grains, one will be able to determine effective elastic properties of their aggregate using the expressions developed for a random packing of spheres. Not only can this theory be directly applied to estimating the acoustical and mechanical properties of basaltic pillows, it is also appropriate for studying the behavior of pelagic sediments when these are composed of hollow grains (for example, diatomites or other microfossils).

Assuming that the compaction of these materials is by grain collapse due to an increase in confining pressure that exceeds their strength, we next derived simple criteria for the collapse of 2-D thick-walled, and thin-walled circular grains. These criteria can be used to estimate the depth of transition between low-velocity (high porosity) and high velocity (low porosity) zones.

PART 3 The interaction of rock grains with friction and slippage is modeled using an analytical solution for plain elastic deformation of cylinders. The model explains the difference between "static" and "dynamic" elastic moduli

2

of natural rock. The numerical experiments performed on a four-grain unit predict the dependence of "static" elastic moduli on confining pressure, on the friction coefficient between grains, and on their initial positions. The "dynamic" elastic moduli depend only on the relative initial positions of the grains and on the confining pressure. Four-grain units with varying initial configurations and friction coefficients can be used for modeling granular material. The "static" and "dynamic" moduli of this material will depend on the statistical distribution of the above-mentioned properties.

PART 4 Prediction of wave propagation in a submarine environment requires modeling the acoustic response of ocean bottom sediments which generally consists of porous granular materials partially or wholly saturated with water. The effect of anisotropy has to be incorporated into the model in order to simulate more realistic responses. Following Biot's theory we present a formulation for seismic wave velocities in a general anisotropic poroelastic medium. We also identify the anisotropic parameters that need to be evaluated or measured for the purpose of estimating the velocities.

The motivation for the work summarized above and appended below has been to understand the physical properties of materials in the upper few hundred meters of the shallow ocean floor (both sediments and basalts). Particularly, we wanted to study the relationship between physical properties (e.g. elastic- wave velocity and attenuation, or strength under load) and the state of the material (micromechanics, porosity, composition and morphology). The approach we chose was to construct simple physical models, isolating these parameters to individually determine their effects on physical properties. The parameters we chose to concentrate on were (1) the geometry of grains and (2) the characteristics of the material at their contacts, which must transmit vibrations and static stresses within the material. In general, it is these properties which control both the initial properties of the materials as they are deposited, and the change of those properties during compaction, lithification, and diagenesis. Five of the six papers we append deal specifically with the development of theories to describe the effects of cement (**Papers 1a and 1b**) and grain geometry (**Papers 2a, 2b, and 3**). The last paper (**Paper 4**) is a summary of Biot theory, which was undertaken to provide a framework for future work in relating our micromechanical models to a generally accepted macroscopic model. This summary, although not at the level of application, is important in defining directions for theoretical work to be undertaken in the future.

3

The application of the theories we developed in the past year to the properties of sediments are (1) to understand the increase of velocity with depth of sediments due to compaction and prior to diagenesis, and (2) to investigate whether mechanical effects may play a role in the abrupt increase in velocity often observed at so-called "diagenetic fronts". After developing a model for the elastic properties of grains with cement (**Paper 1a**), we used this model to calculate the velocities of wave propagation in sediments with three principal components: grains, cement, and fluid-filled pore space. The state of the sediments is controlled by the average number of grain contacts and the properties of those contacts. Two models were developed to study the change of these properties with depth. The first was a simple frictional model with which predictions could be made regarding the behavior of granular materials under load (**Paper 3**), and their recovery upon the removal of load. The second model (**Paper 1b**) allows the construction of an initial material (the sediment as it is deposited) and the prediction of its behavior under steadily increasing load (as it is buried by further sediments). These theories are complementary. Both also allow us to investigate the capability at any depth of such materials to carry static loads (for example, from structures on the seafloor). The latter model predicts, once the material begins to deform, a smooth variation in velocity with depth similar to that presumed by phenomenological models for compaction. However, the compaction rate and hence the rate of change of velocity is determined by the strength of the material between the grains. As this strength can be measured, the model can be tested quantitatively.

One interesting result of these models is that under certain circumstances, materials with a small residual cement layer are stiffer than materials for which the grains are in direct contact at a point. Although this must be investigated more carefully, it does offer an intriguing mechanical explanation for the occasional observation of a high-velocity "layer" at a diagenetic front. A consequence of the frictional model is that the rate of change of velocity is quite modest until the frictional strength of the contacts is exceeded, whereupon a rapid compaction and consequent rapid velocity increase occurs. Again, this mimics the characteristics of a diagenetic front.

Obviously, neither of these overly simple models provides a complete answer. However, each provides useful, testable insights into processes that must occur in compacting sediments. And the rates of change of velocities in each case are controlled by the strengths of the contacts between the grains,

4

whether such contacts are cemented or are free to slip.

Attempts to adapt models of granular materials to the behavior of basalts have previously met with some resistance from members of the scientific community. For example, volcanologists and others feel that the underlying physics is entirely wrong. This is largely because of the conceptual hurdle that must be overcome, because we must adapt the scale so that pillows are the "grains", which are several orders of magnitude larger than grains in sediments. Once these hurdles are overcome, however, the analogies developed through these exercises, which again have been found to be in quantitative agreement with data, can be quite valuable.

With this in mind, we developed a model for the behavior of a cylindrical tube with arbitrary cross-section under load (**Paper 2a**). Such a model was selected because of the common observation that pillow lavas often form as tubes through-which material in passing leaves a frozen shell and a partially evacuated interior. These tubes are often cut by radial cracks generated by cooling stresses. Once the characteristics of these tubes have been determined, construction of an aggregate is straightforward. Again, the aggregate has several useful properties. First, it is substantially "weaker" than the basalt itself, leading to very low elastic-wave velocities. Second, it is capable of rapid velocity increase (and porosity reduction) at a depth corresponding to the collapse pressure of the tubes (**Paper 3b**. One of the principle results of this work is that there is no way to predict the relationship between velocity and porosity for such materials, particularly inasmuch as the properties of the tubes are controlled by the position and number of radial cracks. This model complements our earlier work describing the effects of grain contact stiffnesses in pillows on the properties of the aggregate. Thus the grain contact stiffness results can be incorporated quite naturally into a more complete model for pillows using as a model for the grains the thin-walled hollow cylinder developed under this contract.

The attached summaries and preprints deal primarily with the first phase of this work - that is, development of the models. The next step - application of these models to sediments and basalts, and comparison of the predictions to real data, is now under way. This requires quantitative measurements of the properties of the components of the aggregates. Specifically, we need to know the moduli of the matrix material and of the cement, in the case of the elastic properties measurements, and the yield strength of the cement in the case of the plastic model for compaction. In studying the collapse of

5

basalt pillow tubes, we need to know the strength of the matrix material (basalt). These data are in some cases available in the literature. In the case of basalt strength, however, there is relatively little data, and these measurements are now being made by members of our group.

Over the next several months these results will be incorporated into the models, and the predictions will be tested quantitatively against in situ measurements of velocity. Two papers (one invited) will be presented at the American Geophysical Union Fall 1991 Meeting:

Dvorkin, J. and D. Moos (1991), Seismic velocities in compacting sediments (abstract), EOS, Trans. AGU 72: Fall Meeting 1991 Program and Abstracts.

Moos, D. and J. Dvorkin (1991), Modeling the seismic properties of shallow oceanic crust: Effects of extrusive morphology on seismic velocity (Invited abstract), EOS, Trans. AGU 72 Fall Meeting 1991 Program and Abstracts.

Other publications acknowledging support from this contract include:

Dvorkin, J., Mavko, G. and Nur, A. (1991), The effect of cementation on the elastic properties of granular materials, in press (Mechanics of Materials).

The remaining papers attached to this report will also be modified and submitted for publication.

The Effect of Cementation on the Elastic Properties of Granular Material

Jack Dvorkin, Gary Mavko and Amos Nur

Abstract

A simple analytical model is developed to describe the mechanics of cemented granular material. The two-dimensional problem of the deformation of an arbitrarily-shaped cement layer has been reduced to an ordinary differential equation of the second order. A simple analytical solution is obtained to model the normal and shear deformation of a cement layer with straight boundaries. The problem of the normal compression of two contacting circular elastic grains and an elastic cement layer between them has been reduced to a linear integral equation. This problem has been solved both for two-dimensional (cylindrical grains) and three-dimensional (spherical grains) cases. The elastic modulus of such a combination is strongly increased by cementation compared to the case of a classic Hertzian contact.

Introduction

The acoustic and mechanical characteristics of sedimentary rocks may be strongly affected by the properties and structure of intergranular bond material. The deformational pattern of cement material and its interaction with elastic grains is important for estimates of stress-strain behavior of granular material, as well as for its failure criteria. Sedimentary rocks of interest with intergranular cementation span a wide range from diagenetic sediments and sand-clay mixtures to tar sands.

Numerous publications on the mechanics of granular media were discussed by Stoll (1989). The theoretical description of granular material has been based on the classical solution for the problem of a normal compression of elastic spheres or disks by Hertz (Johnson, 1985) as well as on the results regarding the oblique compression of elastic spheres and disks (Mindlin,

1

1949; Walton, 1978). All these models consider the direct contact of elastic bodies. The dimension of a contact zone changes with varying external forces.

The situation is different for the contact of initially cemented grains. In this case the dimension of a contact zone between two bodies is predetermined and does not change in the process of interaction. Bruno and Nelson (1990) examined the inelastic mechanical behavior of cemented granular material using a two-dimensional discrete element procedure. Intergranular interaction through cementation was modeled using a linear spring scheme.

In this paper we concentrate on the description of cement layer deformation as well as on the interaction of elastic grains with an elastic cement layer. To investigate two-dimensional cement layer deformation when the layer is thin and grains are much stiffer than the cement we have derived a simple analytical model. The approach used is similar to those commonly employed in approximate theories of thin plates and shells. This approach was used by Matthewson (1981) to model an axisymmetric contact on thin compliant coatings. The problem of a two-dimensional arbitrarily-shaped cement layer deformation has been reduced to an ordinary differential equation of the second order. A simple analytical solution has been derived for the case of a cement layer with straight boundaries under compression and shear.

We show that a cement layer under normal compression can be approximately treated as an "elastic foundation" between two grains. Using this result we reduce the two-dimensional problem of interaction between two elastic grains and an elastic cement layer to a linear integral equation. Solving this equation we are able to estimate the elastic modulus of cemented granular material. We also employ the "elastic foundation" approximation to solve the problem of the normal compression of two cemented spherical elastic grains. The presence of a cement layer dramatically increases the elastic modulus compared to the case of an intergranular Hertzian contact.

These theoretical models can be used to predict the influence of cement content and location on the properties of sediments.

Deformation of a Cement Layer

General Equation

To examine the plane deformation of an elastic cement layer we introduce a coordinate system (x, z) in the cross-section of an intergranular boundary

2

(Figure 1). The x axis is directed along the surface of the lower grain; the z axis is directed upward. The problem will be solved in a linear formulation, so that in spite of the possible curvature of the grain surface the x axis can be still considered as being directed along this surface.

Hook's law for the plane theory of elasticity is:

$$\sigma_{xx} = (\lambda + 2\mu)u_x + \lambda w_z,$$

$$\sigma_{zz} = \lambda u_x + (\lambda + 2\mu)w_z, \tag{1}$$

$$\sigma_{xz} = \mu(u_z + w_x).$$

The equations of static elasticity are the following:

$$\frac{\partial \sigma_{xx}}{\partial x} + \frac{\partial \sigma_{xz}}{\partial z} = 0; \quad \frac{\partial \sigma_{xz}}{\partial x} + \frac{\partial \sigma_{zz}}{\partial z} = 0. \tag{2}$$

In equations (1) and (2) σ_{xx}, σ_{zz} and σ_{xz} are normal and shear stresses; u and w are displacements in the x and z directions; lower indexes z and x denote partial derivatives; λ and μ are Lame's constants of the cement.

To find an approximate solution for the problem we assume that the displacements u and w can be expressed in the following form:

$$u(x,z) = \alpha(x)z + \beta(x)z^2; \quad w(x,z) = \epsilon(x)z, \tag{3}$$

where the functions α, β and ϵ are to be found. This assumption can be intuitively validated by the deformation pattern of initially straight fibers of the cement (Fig. 2).

We also assume that the coordinate system (x,z) is connected with the surface of the lower grain, thus displacements $u(x,0) = w(x,0) = 0$ at $z = 0$. The surface of the upper grain moves relative to the lower grain, and displacements u and w are given along this surface:

$$w = W(x); \quad u = U(x)$$

at $z = h(x)$, where $h(x)$ is the thickness of the cement layer.

These boundary conditions lead to the following relations between the functions α, β and ϵ, and known functions $W(x)$, $U(x)$ and $h(x)$:

$$\epsilon(x) = W(x)/h(x); \tag{4}$$

$$\alpha(x) = U(x)/h(x) - \beta(x)h(x). \tag{5}$$

3

Substituting (3) into (1) we arrive at the following expressions for the stresses in the cement layer:

$$\sigma_{xx} = (\lambda + 2\mu)(\alpha'z + \beta'z^2) + \lambda\epsilon,$$
$$\sigma_{zz} = \lambda(\alpha'z + \beta'z^2) + (\lambda + 2\mu)\epsilon, \tag{6}$$
$$\sigma_{xz} = \mu(\alpha + 2\beta z + \epsilon'z).$$

Integrating the first equation (2) in the z direction from 0 to $h(x)$ we arrive at the following relation:

$$\int_0^{h(x)} \frac{\partial}{\partial x}\sigma_{xx}dz + \sigma_{xz}|_{z=h} - \sigma_{xz}|_{z=0} = 0.$$

Substituting expressions (6) into this relation and using (5), we obtain the following equation for the function $\beta(x)$:

$$\beta'' + A(x)\beta' + B(x)\beta = C(x), \tag{7}$$

where

$$A = 6h'/h; \quad B = \frac{3}{h}[h'' - \frac{2(1 - 2\nu)}{h(1 - \nu)}];$$
$$C = \frac{3}{h}[\delta'' + \frac{\epsilon'}{h(1 - \nu)}]; \quad \delta = \frac{U}{h},$$

ν is the Poisson's ratio of the cement.

To set boundary conditions for this equation we will introduce normal force N in the x direction:

$$N = \int_o^h \sigma_{xx}dz = (\lambda + 2\mu)(\alpha'h^2/2 + \beta'h^3/3) + \lambda\epsilon h.$$

This force is assumed to be zero at the left and right sides of the cement layer: $N = 0$ at $x = 0$ and $x = L$, where L is the length of the layer in the x direction.

This assumption leads to the following boundary conditions for the equation (7):

$$\beta' + \beta\frac{3h'}{h} = \frac{6}{h}[\frac{\delta'}{2} + \frac{\epsilon\nu}{h(1 - \nu)}] \tag{8}$$

at $x = 0$ and $x = L$.

The ordinary differential equation (7) can be solved numerically using the boundary conditions (8). Once the functions α and β are computed, stresses σ_{xx}, σ_{zz} and σ_{xz} can be found from relations (6). The resulting normal and shear forces of interaction between two grains are to be computed as the integrals of stresses in the x direction along the cement layer.

4

Special Case - Normal Compression of a Straight Cement Layer

Considering the special case of a straight cement layer under compression we have the following conditions for the functions $U(x)$, $W(x)$ and $h(x)$:

$$U = 0; \ W = const; \ h = const.$$

Equations (7) and (8) become:

$$\beta'' - k^2\beta = 0; \ k = \frac{1}{h}\sqrt{\frac{6(1-2\nu)}{1-\nu}};$$

$$\beta' = C; \ C = \frac{6\epsilon\nu}{h^2(1-\nu)}$$

at $x = 0$ and $x = L$.

Resolving this system we find

$$\beta = \frac{C}{k}\frac{e^{kx}(1 - e^{-kL}) + e^{-kx}(1 - e^{kL})}{e^{kL} - e^{-kL}}.$$

If the length of the cement layer significantly exceeds its thickness ($L \gg h$), we have the following estimates:

$$kL = \frac{L}{h}\sqrt{\frac{6(1-2\nu)}{1-\nu}} \gg 1; \ e^{kL} \gg 1; \ e^{-kL} \ll 1;$$

$$\sigma_{xz}\mid_{z=0} \approx -\frac{\mu W}{h}\sqrt{\frac{6\nu^2}{(1-2\nu)(1-\nu)}}[e^{-k(L-x)} - e^{-kx}].$$

Normal stress in the z direction σ_{zz} can be estimated as follows:

$$\sigma_{zz} \approx (\lambda + 2\mu)W/h.$$

The ratio of maximum shear stress to normal stress γ at the interface of the cement layer is the following:

$$\gamma = \frac{\nu}{1-\nu}\sqrt{\frac{3(1-2\nu)}{2(1-\nu)}}.$$

The maximum value of γ is equal 0.47 at $\nu = 0.4$. Thus, if the friction coefficient between the cement and the grain surface is more than 0.47, the cement layer will not be torn from the grain under normal loading.

5

Special Case - Normal Compression and Shear of a Straight Cement Layer

In this case we consider a shear displacement superimposed on the normal loading. Namely, we put

$$U = const \neq 0; \ W = const; \ h = const.$$

In this case we have the following relations between α and β:

$$\alpha = \delta - \beta h; \ \alpha' = -\beta' h.$$

The equation and boundary condition are identical to the ones in the previous case of pure normal compression. The expression for the normal stress σ_{zz} does not change: $\sigma_{zz} \approx (\lambda + 2\mu)W/h$. Shear stress σ_{xz} is: $\sigma_{xz} = \mu(\delta - \beta h)$ at $z = 0$, and $\sigma_{xz} = \mu(\delta + \beta h)$ at $z = h$. In this case the maximum shear stress at the interface "grain-cement" is approximately:

$$\sigma_{xzmax} \approx \mu\frac{U}{h} + \mu\frac{W}{h}\sqrt{\frac{6\nu^2}{(1 - 2\nu)(1 - \nu)}}.$$

The ratio γ of the maximum shear stress to normal stress is:

$$\gamma = \frac{1 - 2\nu}{2(1 - \nu)}[\frac{U}{W} + \sqrt{\frac{6\nu^2}{(1 - \nu)(1 - 2\nu)}}].$$

In this case parameter γ can be large enough depending on the ratio U/W. Thus, the separation of a cement layer from a grain surface can occur.

Numerical Examples - Tapered Cement Layer; Layer Between Two Circles

In the first example we examined the deformation of a tapered cement layer under normal compression (Fig. 3). The length of the layer is $2\,mm$; the minimal thickness of the layer at its left end is $0.1\,mm$; the tangent of its tilt is 0.2. The elastic constants of the cement are: Young's modulus $E = 2 \cdot 10^9\,Pa$; Poisson's ratio $\nu = 0.3$. The normal displacement of the cement upper surface towards its lower surface is $10^{-4}\,mm$. Average normal and tangential stress distributions along the cement layer are given in Fig. 3. Actual normal stresses (bold curve) are compared with normal stresses computed using an approximate formula of uniaxial deformation: $\sigma_{zz} \approx (\lambda + 2\mu)W(x)/h(x)$ (thin curve). These two curves are very close.

6

In the second example we examined the deformation of a cement layer between two identical circles of a radius $1\,mm$ (Fig. 8, a). The length of the layer is $0.3\,mm$; its minimal thickness is $0.01\,mm$. Elastic constants and compressional displacement are the same as in the first example. Average normal and tangential stress distributions along the cement layer are given in Fig. 4. In this case actual normal stresses (bold curve) are also compared with normal stresses computed using the uniaxial deformation approximation (thin curve). This example also proves the accuracy of approximate uniaxial deformation formula.

These examples show that noticeable shear stresses may develop under normal compression in a cement layer of changing thickness. Normal stresses in such a layer can be approximately calculated using the assumption that the material in every cross-section of the layer deforms uniaxially: $\sigma_{zz} \approx (\lambda + 2\mu)W(x)/h(x)$.

Introducing the Elasticity of Grains - 2D Case

The solution for the problem of two-dimensional deformation of a cement layer between two grains presented above can be incorporated into a more general problem where the deformation of grains is taken into account. The approximate solution of such a problem can be obtained using the result of the previous section:

$$\sigma_{zz} \approx (\lambda + 2\mu)W(x)/h(x). \qquad (9)$$

Assuming as well that shear stresses at grain surfaces do not significantly influence their compressional deformation (Johnson, 1985) we conclude that the concept of "elastic foundation" (*ibid.*) can be used to model the cement layer compressional deformation between two deforming grains (Fig. 5).

Examining the plane deformation of an elastic body on a cement layer - "elastic foundation" - we have the following relation between the displacement of the cement $W(x)$ and the displacement of the body $v(x)$ (Fig. 6):

$$v(x) = \xi + W(x), \qquad (10)$$

where ξ is the rigid translation of the elastic body. Here and below we consider the deformation of the elastic body and the cement layer relative to some fixed rigid surface (Fig. 6) that may be the plane of symmetry between two identical grains (Fig. 8). Assuming that stress distribution in the elastic body is close to one in a half-plane with the identical surface deformation

7

(this assumption is valid provided that the interface "grain-cement" is much smaller than whole grain surface), we arrive at the following relation between the displacement $v(x)$ and normal surface stress $\sigma_{zz}(x)$ (Johnson, 1985):

$$v(x) = \frac{2(1 - \nu_1^2)}{\pi E_1} \int_{-a}^{a} \sigma_{zz}(s) \ln |x - s| ds + const, \qquad (11)$$

where ν_1 is Poisson's ratio and E_1 is Young's modulus of the elastic body; $a = L/2$ is the half-length of the cement layer; the origin of the coordinate system x is in the middle of the cement layer (Fig. 7). Equation (11) implies the linearization of the problem, *i.e.* the assumption that the contact part of the grain surface can be approximated by the interval $|x| < a$ on the x axis.

Substituting (9) and (10) into (11) we arrive at the following integral equation:

$$W(x) = \Lambda \int_{-a}^{a} \frac{W(s)}{h(s)} \ln |x - s| ds + const, \qquad (12)$$

$$\Lambda = \frac{2(1 - \nu_1^2)(\lambda + 2\mu)}{\pi E_1}.$$

This equation can be solved numerically to find function $W(x)$. The constant in the right-hand part of the equation will be calculated using the condition of a given integral compressional force F_c per unit length of cylindrical grains:

$$F_c = \int_{-a}^{a} -\sigma_{zz}(x) dx = \int_{-a}^{a} -\frac{(\lambda + 2\mu)W(x)}{h(x)} dx.$$

Cementation Between Circular Grains

If a cement layer separates two identical circular grains of radius R (Fig. 8, a), its thickness $2h(x)$ is related to coordinate x as follows:

$$h(x) \approx h_0 + \frac{x^2}{2R},$$

where $2h_0$ is the minimal separation between grains. In this case equation (12) has the following form:

$$W(x) = 2R\Lambda \int_{-a}^{a} \frac{W(s)}{nR^2 + s^2} \ln |x - s| ds + const,$$

where $n = 2h_0/R$. A very important special case is the one where grains have a point contact (Fig. 8, b) and, thus, $h_0 = 0$. Equation (12) in this case is:

$$W(x) = 2R\Lambda \int_{-a}^{a} \frac{W(s)}{s^2} \ln|x - s| ds + const. \tag{13}$$

Here we cannot neglect the deformation of grains even if the cement is very soft. If grains are absolutely rigid, this combination will not deform at all. The intriguing question is: how the rigidity of this combination can be compared to the rigidity of two-grain combination without cement between them (Hertzian contact). The principal difference between the example under consideration and the classical Hertzian contact is that in the first case grains will keep a point contact under increasing loading, whereas the Hertzian solution implies the development of a finite contact zone. To answer this question we solved equation (13) numerically using the quadrature method (Delves and Mohamed, 1985).

We examined the deformation of a two-grain combination with cementation between them. The grains of radii $R = 1\,mm$ have a point contact. Young's modulus of grains $E_1 = 2 \cdot 10^{11}$; Poisson's ratio $\nu_1 = 0.3$.

Stress distributions along the grain surface between $x = 0$ and $x = a$ (Fig. 8, b) are given in Fig. 9. In this example ($a = R/3$) we examined eight different cases depending on the ratio of cement to grain stiffness $m = E/E_1$. The Poisson's ratio of the cement was 0.3. The shape of the stress distribution dramatically changes depending on the value of m, whereas the integral of normal stress along the contact interface is constant and equal to the compressive force.

The shape of stress distribution between cemented grains (Fig. 10, bold curve) is completely different from the classical Hertzian case (Fig. 10, thin curve). The dimension of the contact interface between two grains is also different: in the Hertzian case this dimension increases with confining pressure, whereas the contact region between cemented grains remains constant.

To calculate the deformation and the stiffness of the two-grain combination we used the solution for the problem of deformation of an elastic cylinder subjected to external stresses (Novozhilov, 1961). Stress distribution at the grain surface was used to find the deformation of the system under a given confining pressure. The stiffnesses of cemented and noncemented systems are compared in Fig. 11. In this case we used parameters: $m = 0.5$; $a = R/30$. When the confining pressure is small, the stiffness of the cemented system significantly exceeds the stiffness of the Hertzian system. The stiffness of the Hertzian system increases with confining pressure;

9

so does the contact interface. The stiffness of the Hertzian system reaches the stiffness of the cemented system at the confining pressure where the contact interfaces within these two systems become approximately equal. The stiffness of the cemented system does not depend on the confining pressure.

The stiffness of the cemented system for different m and a is compared to the stiffness of the Hertzian system (Fig. 12). The stiffness of the cemented system increases with the length of the cement layer and with the relative stiffness of the cement m. It significantly exceeds the stiffness of the Hertzian system in the range of confining pressure under consideration.

Introducing the Elasticity of Grains - 3D Case

To model the normal compression of two spherical elastic grains interlaid with an elastic cement layer we employ an approach similar to that in a two-dimensional case. Examining the axisymmetrical deformation of a system in a meridional plane (Fig. 8) we assume that normal stresses in a cement layer can be approximated by the "elastic foundation" concept and, therefore, expressed by equation (9): $\sigma_{zz} \approx (\lambda + 2\mu)W(x)/h(x)$, where z is the axis of symmetry and the x axis is placed in the meridional plane. We also use the fact that shear stresses do not significantly influence the compressional deformation of the system (Johnson, 1985). In the case under consideration the displacement of the cement $W(x)$ and normal displacement of a grain surface $v(x)$ are related by equation (10): $v(x) = \xi + W(x)$, where ξ is the rigid translation of a grain.

Following the classical Hertzian solution we assume that stress distribution in the elastic grain is close to one in a half-space with the identical surface deformation. In addition we linearize the problem assuming that the contact region on the grain surface can be approximated by a circle $|x| < a$ in the $z = 0$ plane.

These assumptions lead to the following relation between the displacement $v(x)$ and normal stress at the grain surface σ_{zz} (Timoshenko and Goodier, 1970):

$$v(x) = -\frac{2(1 - \nu_1^2)}{\pi E_1} \int_0^\pi d\varphi \int_0^{x \cos \varphi + \sqrt{a^2 - x^2 \sin^2 \varphi}} \sigma_{zz}(s, \varphi) ds. \quad (14)$$

The integration in this equation is implemented in the $z = 0$ plane, inside the circle $|x| < a$, where a is the radius of the cement layer (Fig. 13); s and φ are the variables of integration.

10

The problem under consideration is an axisymmetrical one, thus the function $\sigma_{zz}(s,\varphi)$ depends only on the r coordinate in the polar coordinate system (r,θ) in the $z = 0$ plane. This argument can be expressed through arguments s and φ as follows: $r = \sqrt{x^2 + s^2 - 2xs\cos\varphi}$. This means that $\sigma_{zz}(s,\varphi) = \sigma_{zz}(r) = \sigma_{zz}(\sqrt{x^2 + s^2 - 2xs\cos\varphi})$. Substituting this expression into equation (14) and using equations (9) and (10) we arrive at the following integral equation for the function $W(x)$:

$$W(x) = -\frac{\Lambda_s}{2R} \int_0^\pi d\varphi \int_0^{x\cos\varphi + \sqrt{a^2 - x^2\sin^2\varphi}} \frac{W(\sqrt{x^2 + s^2 - 2xs\cos\varphi})}{h(\sqrt{x^2 + s^2 - 2xs\cos\varphi})} ds - \xi,$$

where R is the radius of the grain; $\Lambda_s = [4R(1 - \nu_1^2)(\lambda + 2\mu)]/(\pi E_1)$. Using the fact that for the cement layer between two contacting spherical grains $h(x) \approx \frac{x^2}{2R}$, we transform this equation to the following one:

$$W(x) = -\Lambda_s \int_0^\pi d\varphi \int_0^{x\cos\varphi + \sqrt{a^2 - x^2\sin^2\varphi}} \frac{W(\sqrt{x^2 + s^2 - 2xs\cos\varphi})}{x^2 + s^2 - 2xs\cos\varphi} ds - \xi.$$

(15)

The constant ξ in this equation can be calculated using the condition of a given integral compressional force F_c acting on the grains:

$$F_c = \int_0^a -\sigma_{zz}(x)2\pi x\, dx.$$

Equation (15) can be solved numerically similar to equation (13). In this case the quadrature method is applied to the double integral. Once the stress distribution along the grain surface is found, the deformation and the stiffness of the two-grain combination can be calculated. To find the grain surface displacements we used the solution for the problem of deformation of a symmetrically loaded elastic sphere (Lur'e, 1964).

Numerical Examples - Cemented Spherical Grains

We examined the deformation of two contacting identical cemented elastic spheres (Fig. 8., b). All constants were chosen to be identical to those in the 2D case above.

Axisymmetrical stress distributions at the grain surface differ from the Hertzian stress distribution; they are qualitatively similar to the pattern observed in the 2D case.

The stiffness of cemented system is compared to the stiffness of a Hertzian system for different values of m and a/R (Fig. 14). The stiffness of the cemented system does not depend on the confining pressure. It exceeds the stiffness of the Hertzian system at low confining pressure even when the cement is soft and the radius of the cement layer is small.

Conclusions

The two-dimensional problem of deformation of an arbitrarily-shaped cement layer has been reduced to an ordinary differential equation of the second order. A simple analytical solution has been derived for the case of a cement layer with straight boundaries under compression and shear. A cement layer under normal compression can be treated approximately as an "elastic foundation" between two grains. Using this result we reduce the problem of interaction between two elastic grains and an elastic cement layer to a linear integral equation. A cement layer dramatically increases the elastic modulus compared to the case of intergranular Hertzian contact. The shape of stress distribution between cemented grains is completely different from the classical Hertzian case. This shape dramatically changes depending on the ratio of cement stiffness to grain stiffness. The stiffness of the cemented system does not depend on the confining pressure. The stiffness of the cemented system increases with the length of the cement layer and with the relative stiffness of the cement. It significantly exceeds the stiffness of the Hertzian system at low confining pressure. The small increase of the cementation content results in significant growth of a contact zone between two contacting grains and, thus, dramatically increases the stiffness of the system.

REFERENCES

1. Bruno, M.S. and Nelson, R.B.,"Microstructural Analysis of the Inelastic Behavior of Sedimentary Rock," Chevron Oil Field Research Company, 1990.

2. Delves, L.M. and Mohamed,J.L.,"Computational Methods for Integral Equations," Cambridge University Press, 1985.

3. Johnson, K.L.,"Contact Mechanics," Cambridge University Press, 1985.

4. Lur'e, A.I.,"Three-Dimensional Problems of the Theory of Elasticity,"

Interscience Publishers, 1964.

5. Matthewson, M.J., "Axi-Symmetric Contact on Thin Compliant Coatings," Journal Mech. Phys. Solids, Vol. 29, 1981, 89-113.

6. Mindlin, R.D., "Compliance of Elastic Bodies in Contact," Trans. ASME, 71, A-259.

7. Novozhilov,V.V., "Theory of Elasticity," Cambridge University Press, 1961.

8. Stoll, R.D., "Sediment Acoustics," Springer-Verlag, 1989.

9. Timoshenko, S.P. and Goodier, J.N., "Theory of Elasticity," McGraw-Hill, N.Y., 1970.

10. Walton, K., "The Oblique Compression of Two Elastic Spheres," Journal Mech. Phys. Solids, Vol. 26, 1978, 139-150.
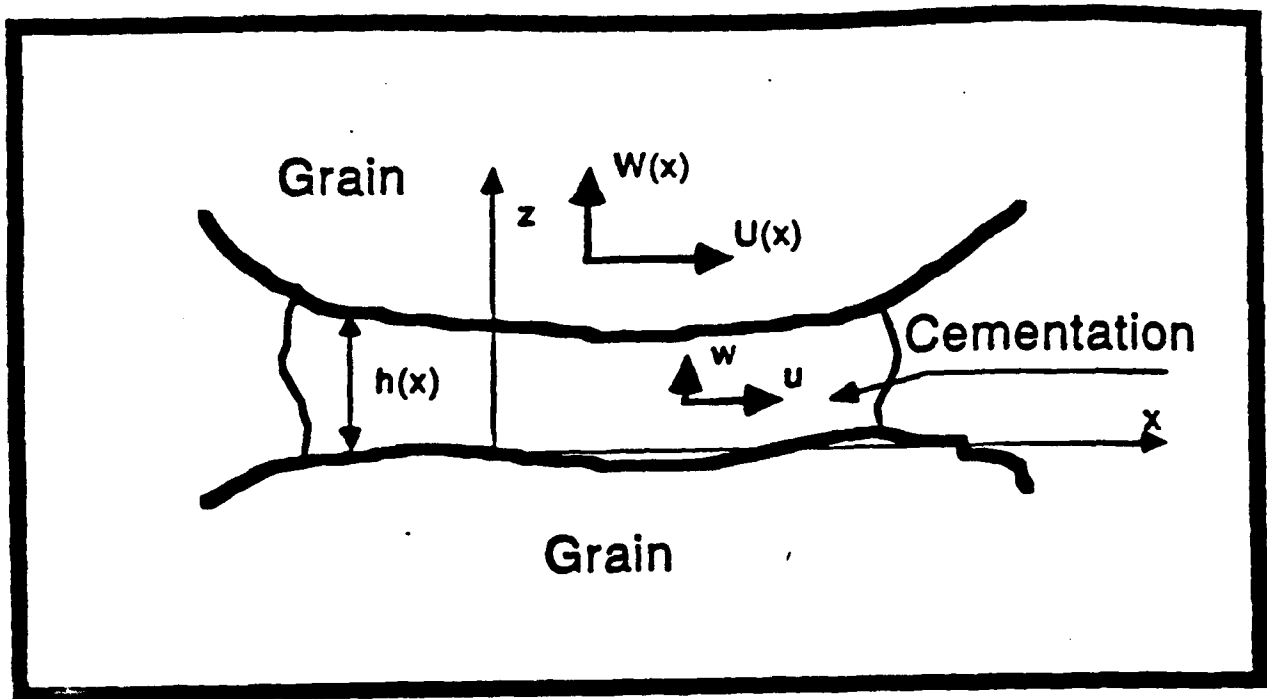
FIGURE 1: Cement layer between two grains.

Deformation
of initialy
straight
fibers
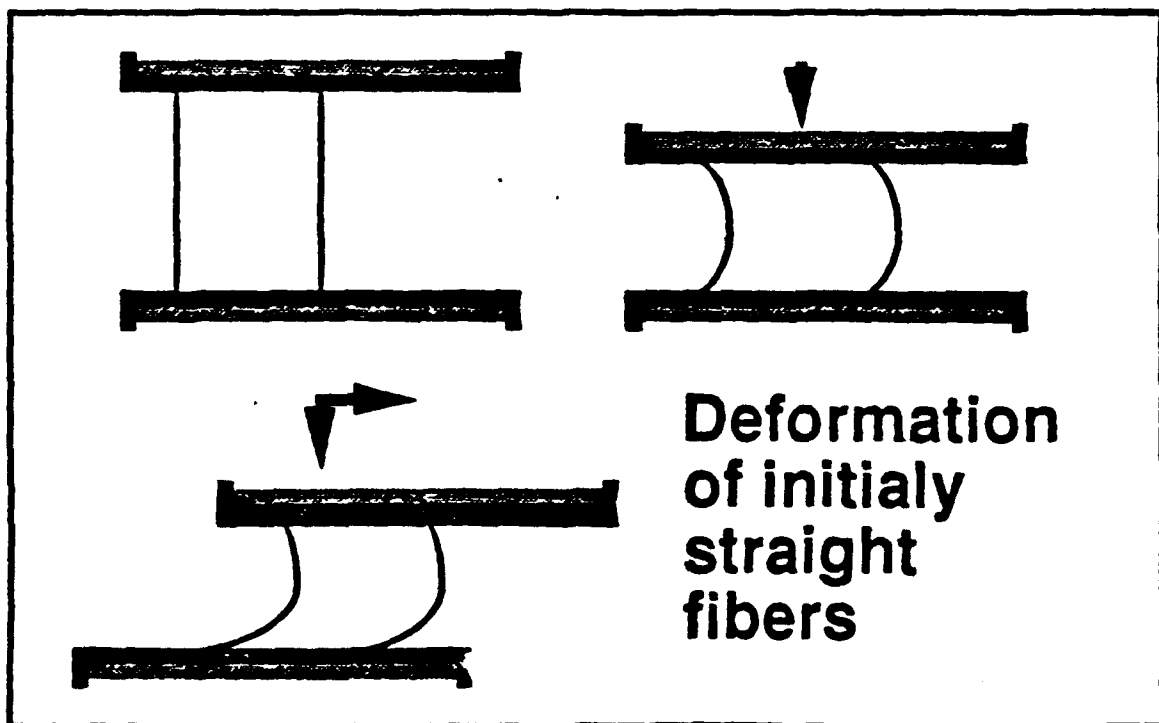
FIGURE 2: Deformation of initially straight fibers in the cement under compression and shear.

STRESS AT THE CONTACT
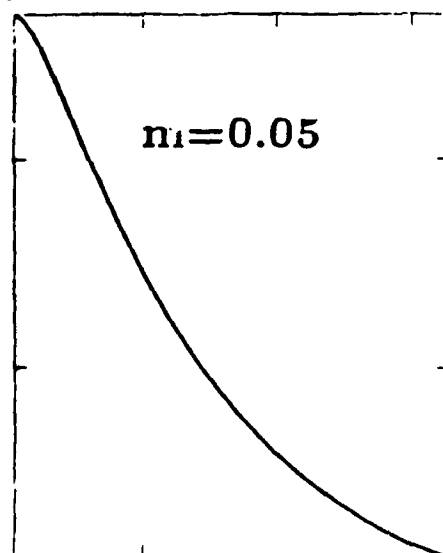
STRESS AT THE CONTACT

FIGURE 3: Average normal and shear stress distributions in the tapered cement layer under normal compression.

FIGURE 4: Average normal and shear stress distributions in the cement layer between two circles under normal compression.

FIGURE 5: Cement layer between two grains as an "elastic foundation."

$$v(x) = \xi + W(x)$$

FIGURE 6: Elastic grain on the cement layer.

FIGURE 7: The deformation of the elastic grain assumed to be close to the deformation of an elastic half-plane.

FIGURE 8: Cementation between two circular grains (cross-section in a two-dimensional case; meridional plane in a three-dimensional case).
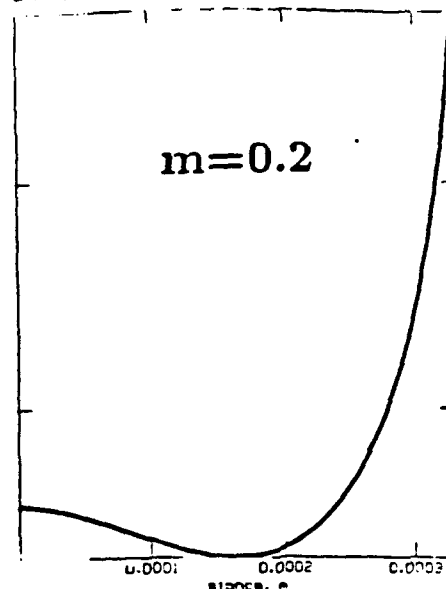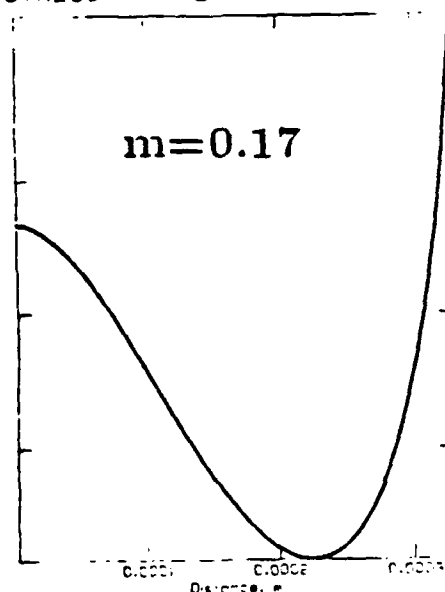
STRESS AT THE CONTACT

m=2.

0.0001   0.0002   0.0003
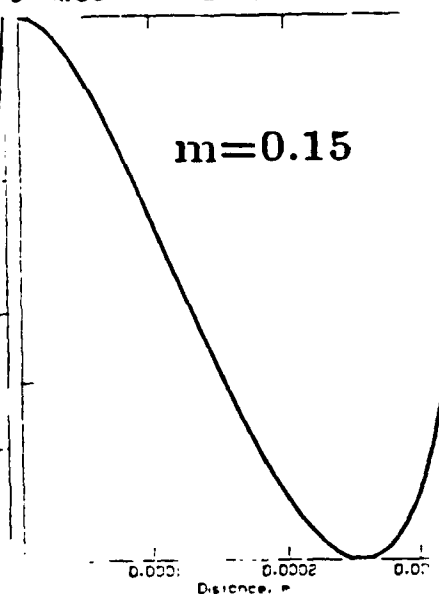Distance, m

STRESS AT THE CONTACT

m=0.7

0.0001   0.0002
Distance, m

STRESS AT THE CONTACT

m=0.2

0.0001   0.0002   0.0003
Distance, m

STRESS AT THE CONTACT

m=0.17

0.0001   0.0002   0.0003
Distance, m

STRESS AT THE CONTACT

m=0.15

0.0001   0.0002   0.0003
Distance, m

STRESS AT THE CONTACT

m=0.1

0.0001   0.0002   0.0003
Distance, m

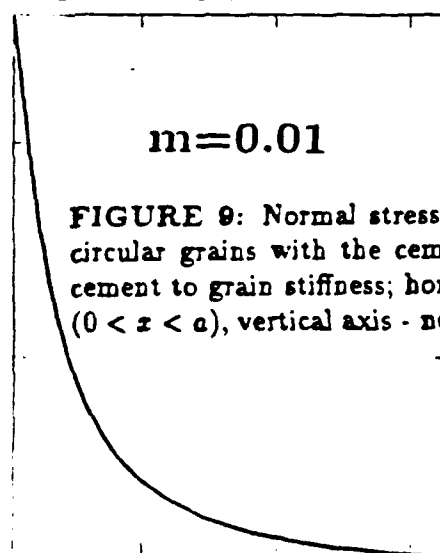STRESS AT THE CONTACT

m=0.05

STRESS AT THE CONTACT

m=0.01

FIGURE 9: Normal stress distribution at the surface of two contactir circular grains with the cement between them depending on the ratio (cement to grain stiffness; horizontal axis - distance along the grain surfac $(0 < z < a)$, vertical axis - normal stress.

STRESS AT THE CONTACT

m=0.01

Hertzian stress distribution

Stress distribution
with cement layer

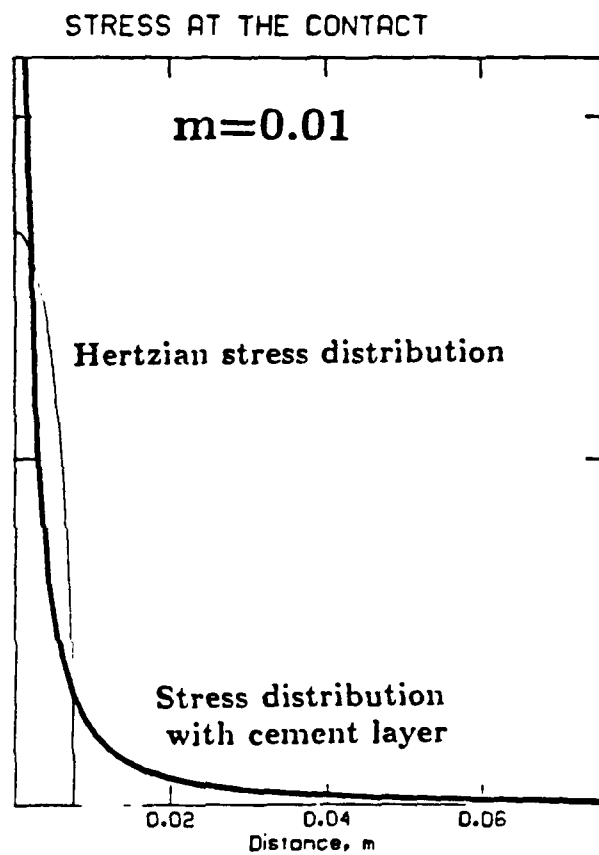0.02   0.04   0.06
Distance, m

FIGURE 10: Normal stress distributions at the surface of two contacting grains with the cement between them (bold curve) and classical Hertzian distribution (thin curve).
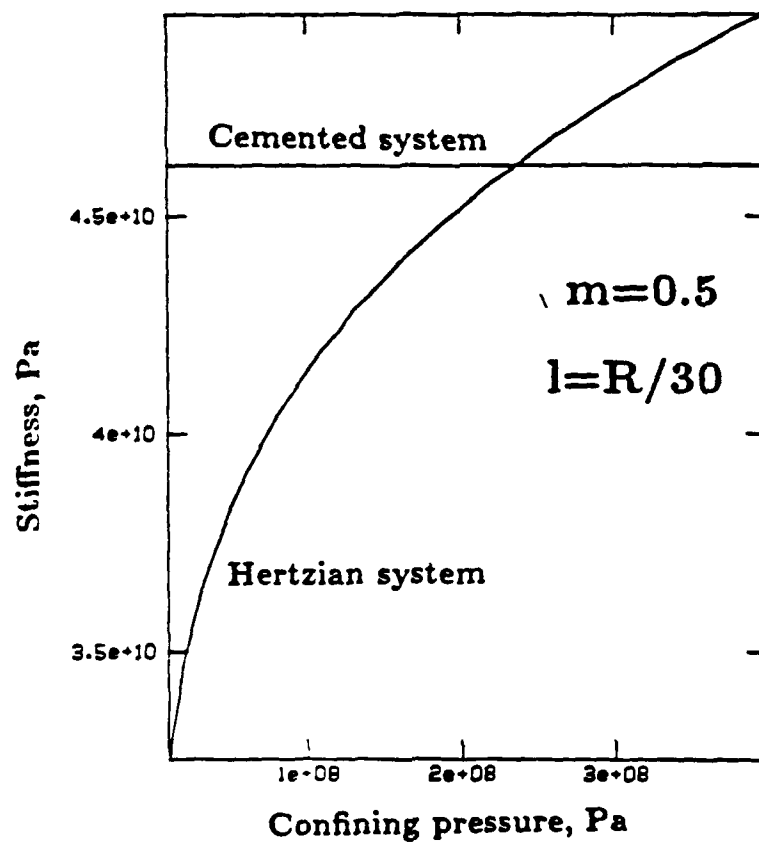
FIGURE 11: The stiffness of cemented and Hertzian systems vs. confining pressure.
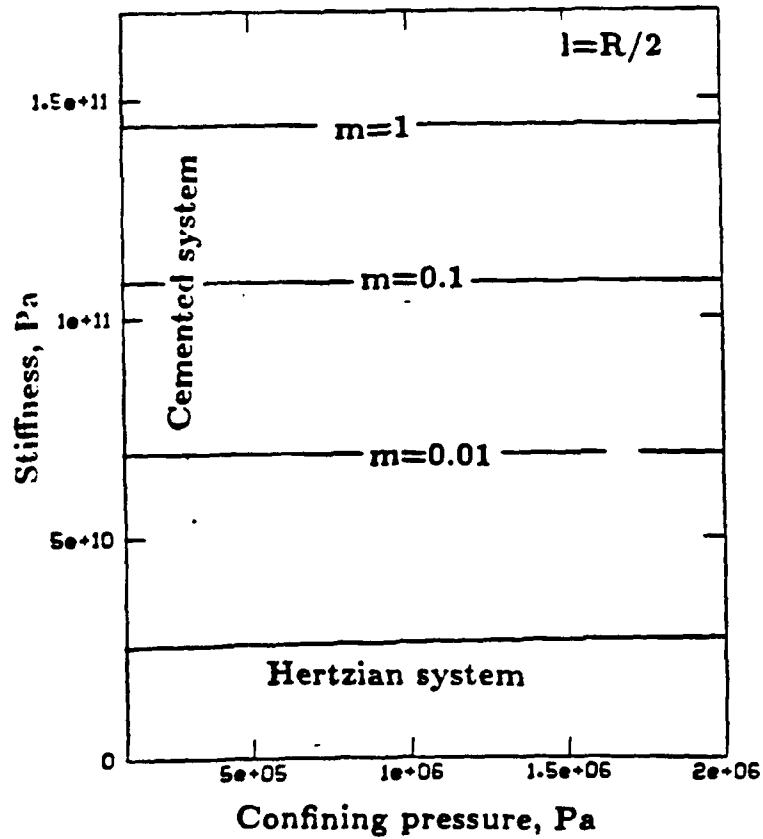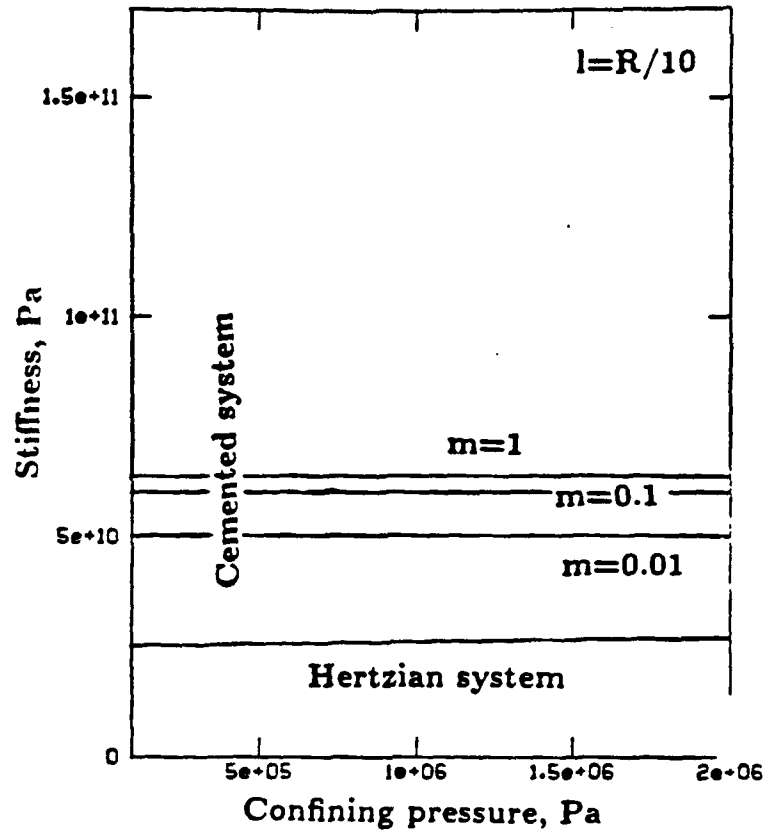
FIGURE 12: The stiffness of cemented and "Hertzian" systems vs. confining pressure depending on the ratio of cement to grain stiffness and on the length of the cement layer.

FIGURE 13: The region of contact on the grain surface $|x| < a$ in the plane $z = 0$.

FIGURE 14: The stiffness of cemented spheres systems and Hertzian systems vs. confining pressure depending on the ratio of cement to grain stiffness and on the length of the cement layer.
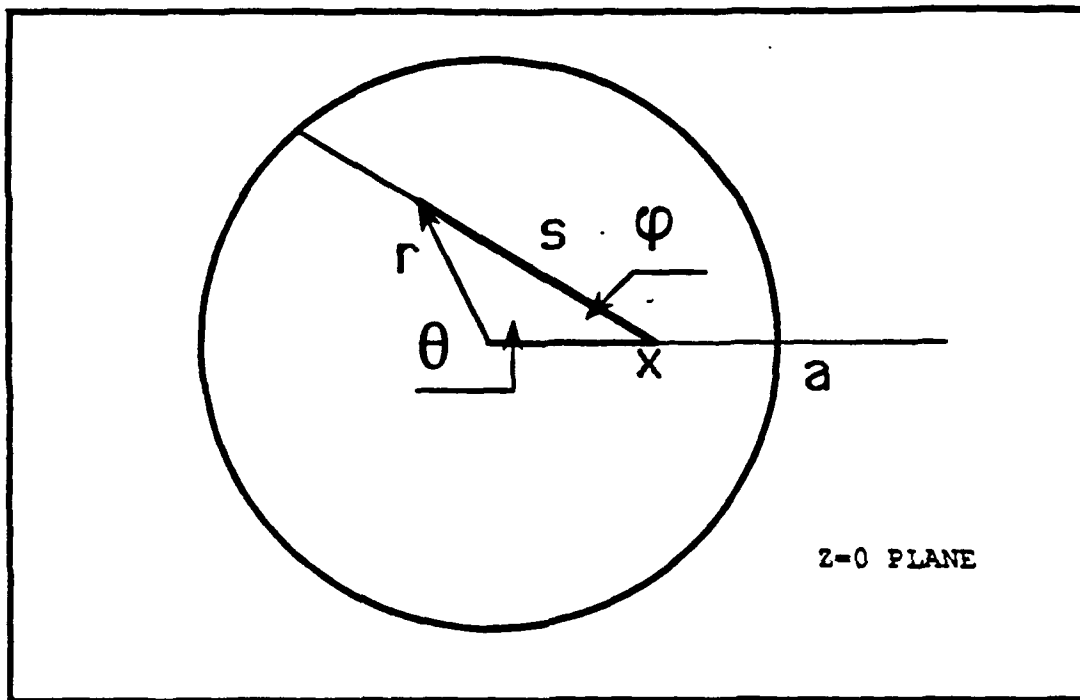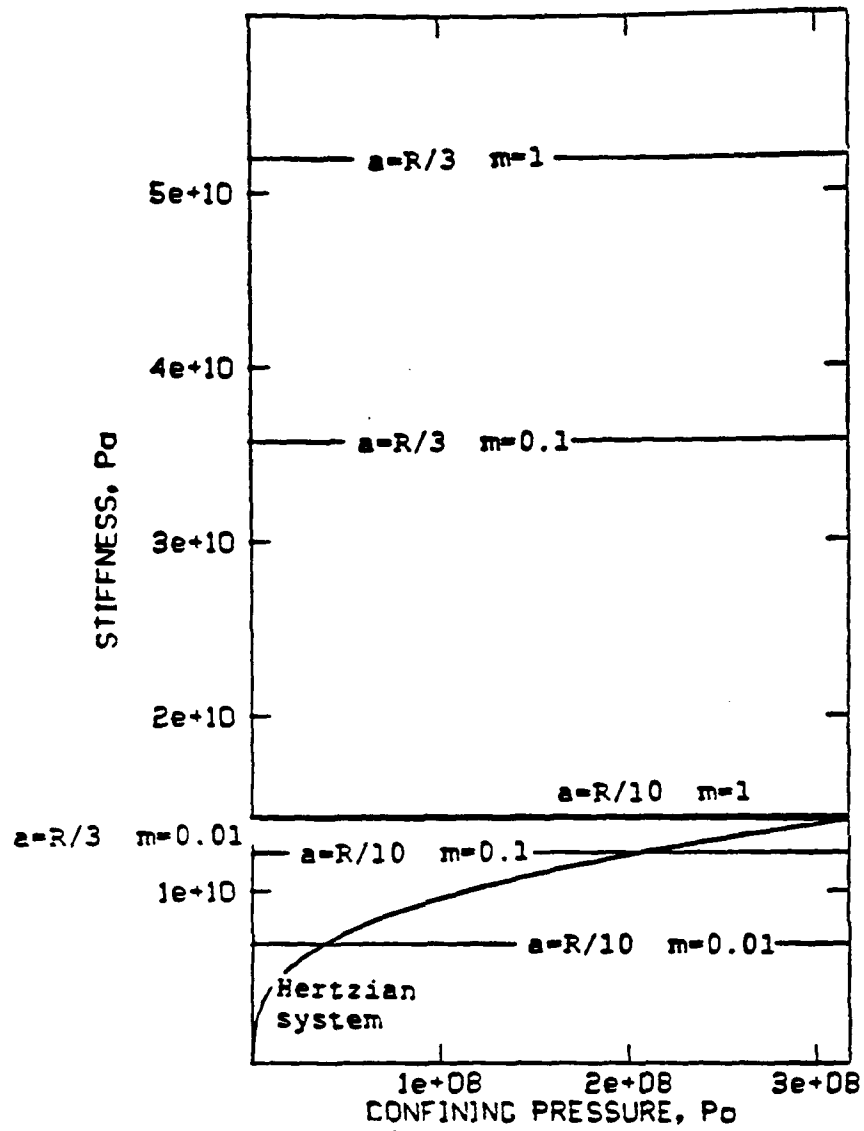
Seismic Velocities in Compacting Sediments

Abstract

We present a theoretical model for the compaction of sediments formed by quartz grains separated at their contacts by a cementing component. Compaction occurs due to lithostatic pressure that results in increasing contact stresses with burial. As the stresses at the contact become larger, the cementing material yields, the separation between the grains decreases, and the area of the cemented contact increases. This results in an increase in P- and S-wave velocity with depth. The rate of increase depends on the strength of the cement. Similarly, the rate of porosity reduction, which is *dependent on the reduction of separation of* the grains, also depends on the strength of the cement. Although the compaction of the sediment occurs due to plastic yield of the cementing component, the material as a whole behaves elastically in response to seismic wave excitation. Our estimates of the seismic properties of compacting sediments are based on the theory of cemented granular material (Dvorkin et al., 1991) that is used to compute the contact stiffness of cemented grains. Seismic velocities are evaluated using standard formulas that relate the elastic properties of granular materials to the contact stiffness and the average number of contacts per grain. The results indicate that the velocities steeply increase on the initial stage of compaction. As compaction continues, the velocities gradually approach constant values that correspond to the direct contact of the grains. If the cement is extremely soft relative to the grains, a velocity maximum occurs just prior to the pressure at which the grains contact. Our theoretical predictions agree qualitatively with velocity-depth profiles within oceanic sediments.

Introduction

In this paper we develop a theory for the compaction of granular sediments due to increasing lithostatic pressure. We assume that rigid grains are sep-

1

arated by a cementation material that is being pushed out of grain contacts as confining pressure increases. Using simple yield criterion we find the separation between grains and the size of the cemented zone at the grain contacts. The knowledge of the geometry of the grain contacts allows us to apply our theory of cemented elastic grains (Dvorkin et al., 1991). Then we use formulas that relate acoustic velocities in random sphere packs to the normal and tangential contact stiffnesses and the number of contacts per grain (Winkler, 1983).

It is important to mention that in spite of the plastic regime of the compaction of sediments, we assume that they react elastically to the seismic wave excitation.

In addition we give approximate formulas for velocities in cemented sediments obtained under the assumption that grains are absolutely rigid.

Plastic Compaction of Granular Sediments

We assume that two adjacent spherical grains are separated at their contact by a given constant amount of cementing material. As contact pressure increases, cement is being pushed out of the contact zone. This process results in smaller intergranular separation and increasing area of the cemented contact zone (Fig. 1).

We use the following simple speculation in order to find the geometry of the cemented contact zones as a function of the confining pressure. If the confining pressure is P_c then the total force F_t acting upon the surface of a spherical grain of radius R is $F_t = 4\pi R^2 P_c$. This force, if distributed among C contacts, produces a forces per contact $F_c = F_t/C = 4\pi R^2 P_c/C$.

The average normal stress σ in a cement disk of central angle θ_0 (Fig. 2) is:

$$\sigma = \frac{F_c}{\pi(R\theta_0)^2} = \frac{4P_c}{C\theta_0^2}.$$

This formula allows us to relate central angle θ_0 to the confining pressure and the yield limit of the cement σ_s:

$$\theta_0 = 2\sqrt{\frac{P_c}{C\sigma_s}}. \tag{1}$$

2

Compaction and the Contact Geometry

The half volume of the cement disk of central angle θ (Fig. 2) is:

$$V_c = \pi R^3 \theta_0^2 \left(\frac{h_0}{R} + \frac{\theta_0^2}{4} \right),$$

where h_0 is the half-distance between two adjacent grains.

Assuming that the volume of the cement at the contacts does not change with compaction and is given by the constant ratio of cement to grain volume k_v, we find that the total volume of cement per grain is

$$V_{cem} = k_v \frac{4}{3} \pi R^3.$$

Thus the volume V_c can be calculated as

$$V_c = \frac{V_{cem}}{C} = k_v \frac{4 \pi R^3}{3C}.$$

Now the half-distance between two adjacent grains h_0 can be related to the radius of a grain R as:

$$\frac{h_0}{R} = \frac{4 k_v}{3 C \theta_0^2} - \frac{\theta_0^2}{4}. \tag{2}$$

Equations (1) and (2) determine the geometry of the cementation at the contact depending on the confining pressure. Given this geometry, the normal contact stiffness of two spherical grains can be calculated using our theory of intergranular cementation (Dvorkin et al., 1991).

Seismic Velocities and Contact Stiffnesses

To find seismic velocities V_p and V_s as functions of confining pressure we use formulas relating V_p and V_s to the normal and tangential contact stiffnesses S_n and S_t (Winkler, 1983):

$$V_p^2 = \frac{3C}{20 \pi R \rho} \left(S_n + \frac{2}{3} S_t \right), \quad V_s^2 = \frac{C}{20 \pi R \rho} \left(S_n + \frac{3}{2} S_t \right), \tag{3}$$

where ρ is the density of the grain material. These formulas were derived for the random packing of identical elastic spheres. Stiffness is defined as

3

the ratio of an acting force to the displacement it produces. A convenient interpretation of (3) in terms of bulk and shear moduli K and G is:

$$K = \frac{C}{12\pi R}S_n, \ G = \frac{C}{20\pi R}(S_n + S_t). \tag{4}$$

Seismic velocities can be expressed through K and G as:

$$V_p = \sqrt{\frac{K + 4G/3}{\rho_r}}, \ V_s = \sqrt{\frac{G}{\rho_r}}, \tag{5}$$

where ρ_r is the density of the rock.

Given the Poisson's ratio of the rock ν, the shear modulus G can be expressed through the bulk modulus K as:

$$G = K\frac{3(1 - 2\nu)}{2(1 + \nu)}. \tag{6}$$

Formulas (4) - (6) can be used to calculate V_p and V_s given the normal stiffness of two grains and the Poisson's ratio.

Seismic Velocities and Confining Pressure

In this section we use the solution for the problem of the normal compression of cemented circular grains (Dvorkin et al., 1991) in order to find V_p and V_s versus confining pressure P_c. The order of calculating the velocities is the following:

equation (1) is used to find θ_0 as a function of P_c;

equation (2) is used to find the half-distance h_0;

results of Dvorkin et al. (1991) are used to find normal stiffness S_n;

the bulk modulus K is calculated from (4);

a certain value is assigned to the Poisson's ratio ν of the rock;

formulas (6) and (5) are used to calculate G, and V_p and V_s.

The results of calculations with $\nu = 0.3$ are presented in Fig. 3. Different curves V_p-P_c and V_s-P_c were obtained for various values of ratio $m = E_c/E_g$, where E_c and E_g are the Young's moduli of the grain material and the cement. We also varied the amount of cement in the rock (parameter k_v).

Plots of V_p and V_s versus P_c for the case where $m=0.07$ $k_v=0.2$ are presented in Fig. 3A. Velocities steeply increase on the initial stage of compaction. As compaction continues, the velocities gradually approach constant values that correspond to the direct contact of grains. Fig. 3B gives

4

plots of V_p and V_s versus P_c for $m=0.07$ $k_v=0.1$. Velocities here are smaller than in the first examle, that is due to reduced amount of the cementation.

An interesting effect of peaks in P- and S-velocity before they reach their constant values is shown in Fig. 3C. In this case the cementation is very soft compared to the grain material ($m=0.01$) and $k_v=0.1$. This is due to the fact that the normal stiffness of two spherical grains separated by a thin layer of a soft cement can be higher than that of directly contacting grains.

Our theoretical predictions have a qualitative agreement with velocity measurements in oceanic sediments.

Simplified Formulas for S_n and S_t

Simple formulas for evaluating the contact stiffnesses of two cemented grains can be obtained under the assumption that the grains are absolutely rigid. These formulas can be applied only if the cementation is very soft compared to the material of the grains and if grains are not in the direct contact.

In the following derivations we use the result of Dvorkin et al. (1991) that a cement layer can be treated approximately as an elastic foundation. Namely, we assume that a normal stress in the cement layer (in the direction perpendicular to the surface of the grain) is:

$$\sigma = (\lambda + 2\mu)W/h, \tag{7}$$

where W is the displacement of the cement normal to the grain surface; h is the thickness of the cement layer between two grains; and λ and μ are Lame's constants of the cement.

For the shear stress τ we will use the following formula:

$$\tau = \mu U/h, \tag{8}$$

where U is the tangential displacement between two grains.

The thickness of the cementation between two circular grains is (Fig. 2):

$$h(x) = 2(h_0 + \frac{x^2}{2R}). \tag{9}$$

From (8) and (9) we find that

$$\tau(x) = \frac{\mu U}{h(x)} = \frac{\mu U R}{x^2 + 2Rh_0}.$$

5

The resulting tangential force T between two grains produced by the displacement U is for the 2-D case:

$$T = 2 \int_0^{x_0} \tau(x)dx = \mu U \sqrt{2R/h_0} \arctan(\frac{\theta_0}{\sqrt{2}}\sqrt{R/h_0}).$$

The normal force produced by the displacement W can be found from (7):

$$N = (\lambda + 2\mu)W\sqrt{2R/h_0} \arctan(\frac{\theta_0}{\sqrt{2}}\sqrt{R/h_0}).$$

These formulas can be used now to find the normal and tangential stiffnesses between two grains for the two-dimensional case:

$$S_t = T/(U/2) = 2\mu\sqrt{2k}\arctan(\theta_0\sqrt{k/2}),$$

$$S_n = N/(W/2) = 2(\lambda + 2\mu)\sqrt{2k}\arctan(\theta_0\sqrt{k/2}),$$

where $k = R/h_0$.

For the 3-D case of two cemented spherical grains we have:

$$T = \int_0^{x_0} 2\pi x \tau(x)dx = \pi\mu U R\ln(1 + \frac{\theta_0^2}{2}k),$$

$$N = \pi(\lambda + 2\mu)WR\ln(1 + \frac{\theta_0^2}{2}k),$$

$$S_t = 2\pi\mu U \ln(1 + \frac{\theta_0^2}{2}k), \tag{10}$$

$$S_n = 2\pi(\lambda + 2\mu)R\ln(1 + \frac{\theta_0^2}{2}k). \tag{11}$$

Velocities V_p and V_s can be calculated now from (3).

Formulas (10) and (11) can be used only for the rough, an order of magnitude estimates of seismic velocities.

Conclusions

We developed a theoretical model for the compaction of sediments formed by rigid grains separated at their contacts by a cementing component. Compaction occurs due to lithostatic pressure that results in increasing contact stresses with burial. Our estimates of the seismic properties of compacting

6

sediments are based on the theory of cemented granular material that is used to compute the contact stiffness of cemented grains. The compaction of sediments occurs as a plastic process but they react elastically to the seismic wave excitation. Velocities V_p and V_s steeply increase on the initial stage of compaction. As compaction continues, the velocities gradually approach constant values that correspond to the direct contact of grains. An interesting effect of smooth peaks in P- and S-velocity before they reach their constant values is predicted if cementation is very soft compared to the grain material (e.g. quartz grains in silt). Our theoretical predictions have a qualitative agreement with velocity measurements in oceanic sediments.

References

1. Dvorkin, J., Mavko, G. and Nur, A., "The Effect of Cementation on the Elastic Properties of Granular Material," 1991, in press (Mechanics of Materials).

2. Winkler, K., "Contact Stiffness in Granular Porous Materials: Comparison between Theory and Experiment," 1983, GRL, 10 (11), 1073-1076.
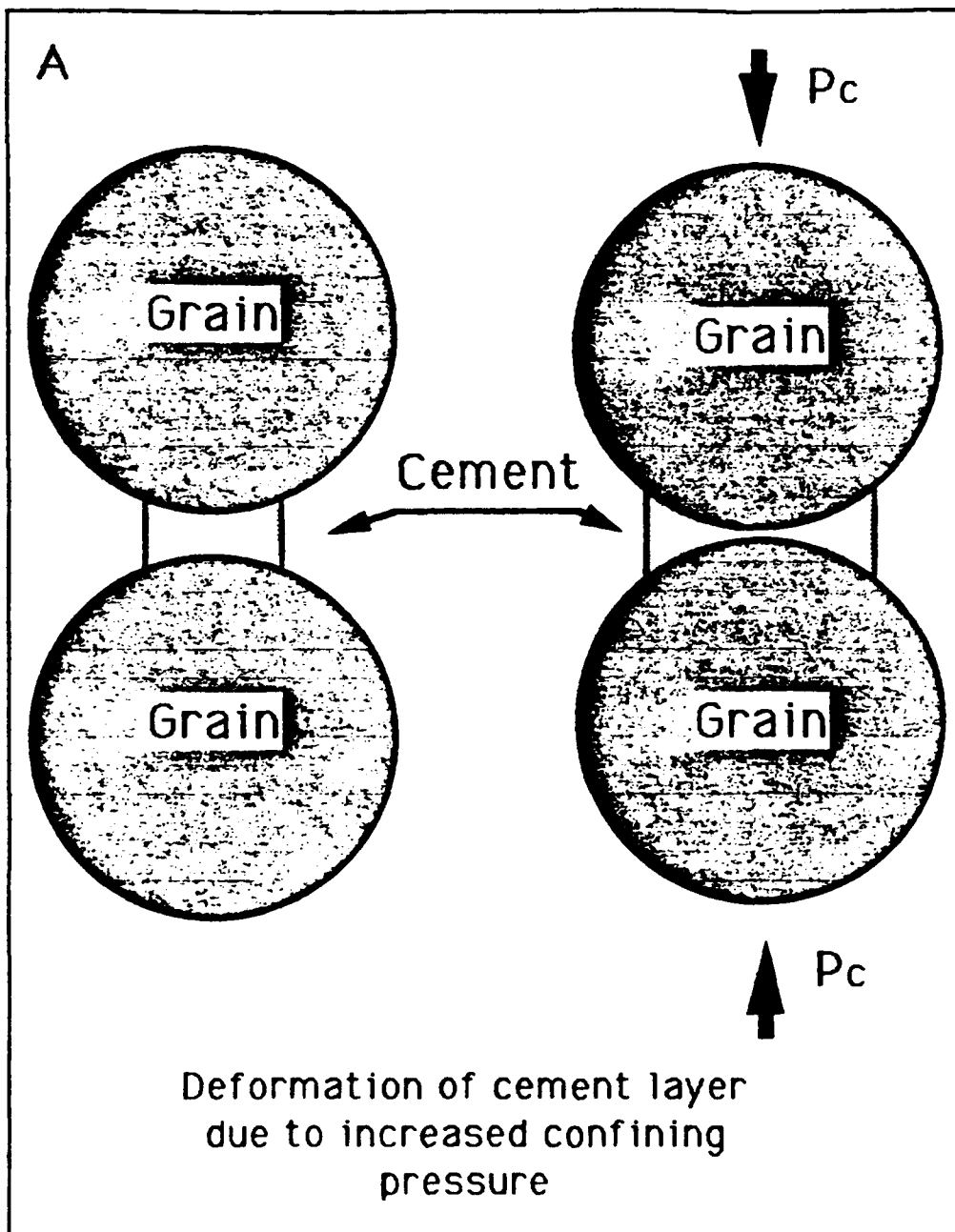
Figure 1 : Deformation of the cementation between two spherical grains due to increasing confining pressure.
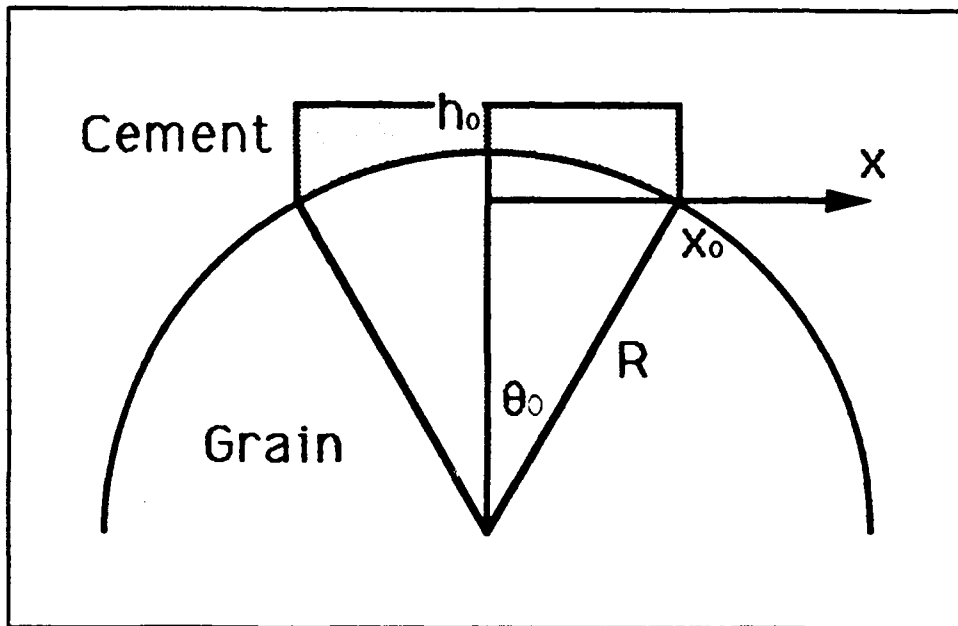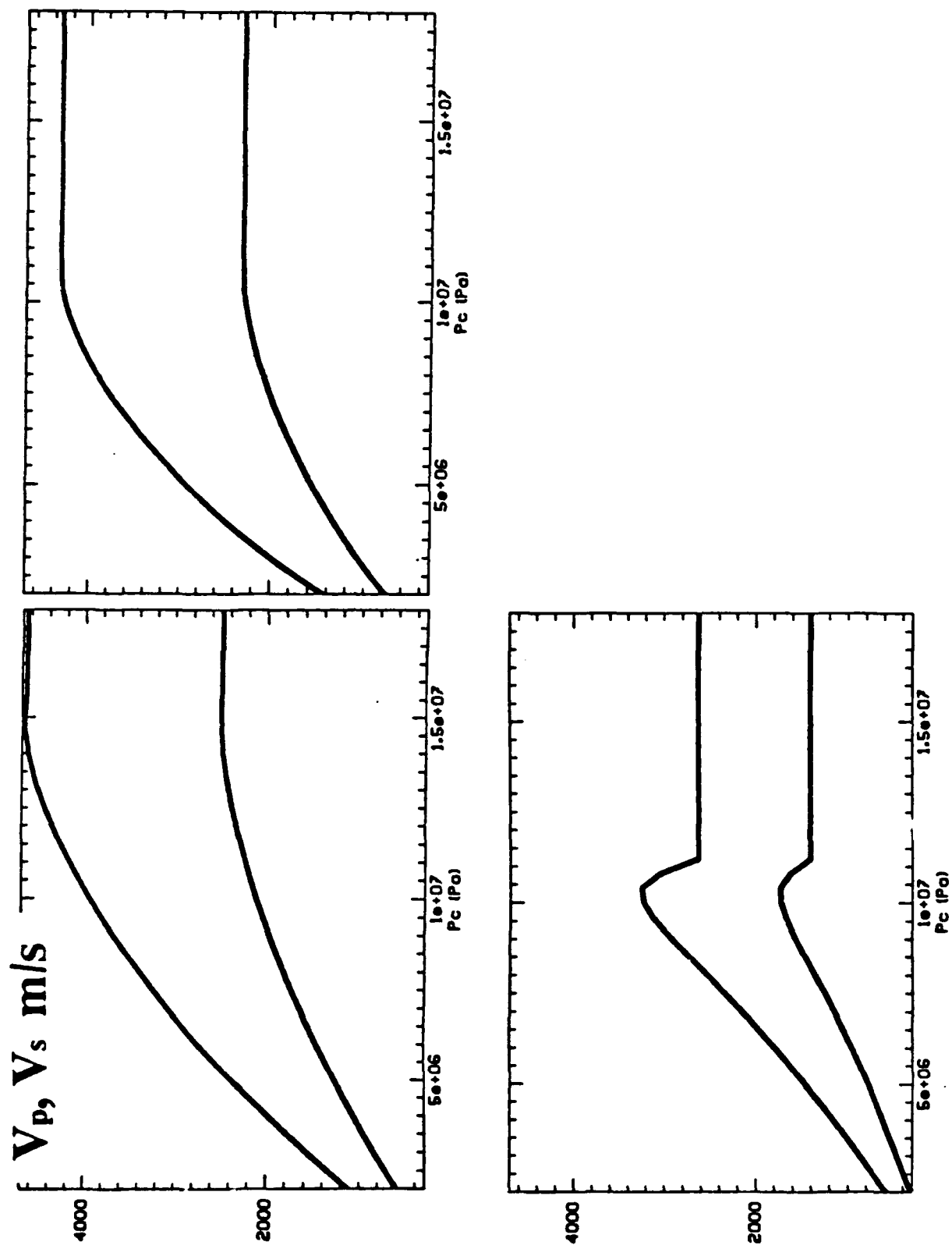
Figure 2 : Cementation layer on a spherical grain.

Figure 3 : V_p (bold curves) and V_s (thin curves) versus confining pressure P_c. A. $k_v = 0.2$, $m=0.07$; B. $k_v=0.1$, $m=0.07$; C. $k_v=0.1$, $m=0.01$.

Seismic Velocities in Compacting Sediments

Jack Dvorkin and Daniel Moos (both at: Department of Geophysics, Stanford University, Stanford, CA 94305)

We present a theoretical model for the compaction of sediments formed by quartz grains separated at their contacts by a cementing component. Compaction occurs due to lithostatic pressure that results in increasing contact stresses with burial. As the stresses at the contact become larger, the cementing material yields, the separation between the grains decreases, and the area of the cemented contact increases. This results in an increase in P- and S-wave velocity with depth. The rate of increase depends on the strength of the cement. Similarly, the rate of porosity reduction, which is dependent on the reduction of separation of the grains, also depends on the strength of the cement.

Although the compaction of the sediment occurs due to plastic yield of the cementing component, the material as a whole behaves elastically in response to seismic wave excitation. Our estimates of the seismic properties of such a material are based on the theory of a cemented granular material (Dvorkin, et al., 1991) that is used to compute the contact stiffness of cemented grains. Seismic velocities are evaluated using standard formulas that relate the elastic properties of granular materials to the contact stiffness and the average number of contacts per grain.

The results indicate that the velocities increase rapidly on the initial stage of compaction. As compaction continues, the velocities approach constant values that correspond to the direct contact of the grains. If the cement is extremely soft relative to the grains, a velocity maximum occurs just prior to the pressure at which the grains contact. Our theoretical predictions agree qualitatively with velocity-depth profiles within oceanic sediments. However, the importance of these effects depends on the strengths of the materials involved.

Dvorkin, J., Mavko, G. and Nur, A., 1991, The Effect of Cementation on the Elastic Properties of Granular Material, Mechanics of Materials, in press.

Modeling the Granular Structure of Rocks

Abstract

The interaction of rock grains with friction and slippage is modeled using an analytical solution for plain elastic deformation of cylinders. The model explains the difference between "static" and "dynamic" elastic moduli of natural rock. The numerical experiments performed on a four-grain unit predict the dependence of "static" elastic moduli on confining pressure, the friction coefficient between grains and their relative initial positions. The "dynamic" elastic moduli depend mainly on the relative initial positions of grains and confining pressure.

Four-grain units with varying initial configurations and friction coefficients can be used for modeling granular material. The "static" and "dynamic" moduli of this material will depend on the statistical distribution of the above-mentioned properties.

Introduction

The theoretical description of granular material regarding the mechanical behavior of natural rock has been a published subject for more than 30 years. In many publications the authors employed regular packing of spherical grains (Gassman, 1951, Duffy and Mindlin, 1957, Deresiewicz, 1958, White, 1965, Walton, 1975).

Digby (1981) investigated the behavior of identical, randomly stacked, spherical particles. Contacting particles are initially bonded together across small areas. The solution predicts the dependence of elastic wave speeds on the confining pressure and adhesion radii of contacting particles.

Walton (1987) derived the effective incremental elastic moduli of random packing of identical elastic spheres. The spheres are assumed to be either infinitely rough or perfectly smooth. The results derived are applicable to dense packing.

Our goal is to examine the deformation of unconsolidated rocks under different types of loading conditions. Using the exact analytical solution for the deformation of an elastic cylinder under arbitrary external forces distributed along its perimeter (Novozhilov, 1961) we model the interaction of circular grains with friction and slippage. Employing the simple combination of four identical circular grains we explain the observed difference between "static" and "dynamic" elastic moduli of unconsolidated rocks assuming that in the later case no slippage occurs. Considering frictional forces we explain the hysteresis effect in stress-strain relationships for granular materials.

Deformation of Circular Cylinder

The solution of the plane problem for a circular cylinder (Novozhilov, 1961) is based on the general theory derived for plane deformation of elastic bodies. Here we use the following relationship between displacements u and v and complex functions $\varphi(z)$ and $\psi(z)$ in a complex plane $z = x + iy$ (Fig. 1):

$$u + iv = \frac{1+\nu}{E}[\Lambda\varphi(z) - z\overline{\varphi'(z)} - \overline{\psi(z)}], \tag{1}$$

where E and ν are the Young's modulus and Poisson's ratio of the cylinder; $\Lambda = 3 - 4\nu$; $\overline{\varphi'(z)}$ and $\overline{\psi(z)}$ are functions conjugate with respect to $\varphi'(z)$ and $\psi(z)$.

The complex functions $\varphi(z)$ and $\psi(z)$ can be found using boundary conditions for normal f_ρ and tangential f_θ traction on the cylinder perimeter.

The functions $\varphi(z)$ and $\psi(z)$ are regular within the region under consideration, and can be represented in the form of power series

$$\varphi(z) = \sum_{k=1}^{\infty} \frac{\alpha_k}{R^k}z^k, \quad \psi(z) = \sum_{k=1}^{\infty} \frac{\beta_k}{R^k}z^k, \quad \varphi'(z) = \sum_{k=1}^{\infty} k\frac{\alpha_k}{R^k}z^{k-1}. \tag{2}$$

The coefficients α_k and β_k are connected with the boundary tractions as follows:

$$\alpha_1 = A_1/2; \quad \alpha_k = A_k, \ k > 1; \quad \beta_k = \overline{A_{-k}} - (k+2)A_{k+2}.$$

$$A_k = \frac{R}{2\pi k}\int_0^{2\pi} (f_\rho + if_\theta)\exp[-i(k-1)\theta]\,d\theta.$$

Here R and θ are the modulus and argument in the complex z plane.

2

Conditions at Grain Contact

To describe a normal stress distribution along contact surfaces we use the Hertzian approach (Johnson, 1984). The contact stripe between two cylinders pressed against each other by a force N has a width $2a$, where

$$a^2 = \frac{4NR_c(1 - \nu^2)}{\pi E};$$

(3)

and R_c is the cylinder radius.

Pressure distribution along the contact surface can be presented in the following form:

$$f_\rho(\xi) = \frac{2N}{\pi a^2}\sqrt{a^2 - \xi^2},$$

(4)

where ξ is the local coordinate system (see Fig. 2).

To model the distribution of a tangential traction along the contact surface of two cylinders when slippage occurs we use the Coulomb law of friction:

$$f_\theta = \kappa f_\rho,$$

where κ is the coefficient of sliding friction.

The modeling of tangential traction distribution in the absence of sliding is more complicated. Mindlin's (1954) solution of this problem predicts that if two spheres are pressed together by a constant normal force and then tangential forces are applied, the pattern of normal traction remains unchanged while the resulting distribution of tangential tractions tends to infinity at the periphery of the contact area. Since infinite stresses are not physically possible, stress relief in the region of stress concentration is allowed. This effect gives rise to a tangential traction distribution that is not proportional to the normal traction.

Walton (1987) obtained part of the solution corresponding to shear using the assumption of perfect adhesion: that is, no relative slip between the two spheres is allowed over the contact area, while the final state is being attained. The resultant configuration and the occurence of slippage are strongly dependent on whether the two spheres are first compressed and then sheared or whether the two motions are occuring simultaneously. In this case the tangential traction distribution has a form similar to the one given by Eqn. 4. In this case if slippage occurs, it will be in the form of sliding over the whole of the contact area.

3

In our model we use Walton's solution for the shear traction distribution:

$$f_\theta(x) = \frac{2T}{\pi a^2}\sqrt{a^2 - \xi^2}, \tag{5}$$

where T is the resulting tangential force applied to the contact area.

The dimensions of the contact area between two cylinders is usually very small compared to cylinder size. This allows us to use in this case Saint-Venant's principle, according to which statically equivalent systems of forces distributed over a small part of the boundary of an elastic body produce in the body systems of stresses which differ from each other only in the immediate vicinity of the area of loading. However, at sufficient distances from this area, the stresses aroused by one or the other system of forces are practically identical. Thus, under certain conditions the form of shear traction distribution is not really important to compute the resulting deformation of cylindrical grains.

Four Cylinders System - Active and Reactive Forces

To understand the peculiarities of grain interaction we examine a simple combination of four identical cylinders (Fig. 3A) subjected to the internal loadings P_1 and P_2.

The equilibrium condition of four cylinders system can be presented in the following form:

$$P_1 = 2(N\cos\alpha + T\sin\alpha), \quad P_2 = 2(N\sin\alpha - T\cos\alpha), \tag{6}$$

where N and T are the normal and tangential reactive forces acting between two cylinders (Fig. 3B); α is an angle defining the relative position of the cylinders.

When slippage occurs the relationship between N and T is defined by the Coulomb law of friction: $|T| = \kappa N$. When there is no relative motion between two cylinders the reactive forces are connected by the following formula: $|T| < \kappa N$. Making use of Eqn. 7 we arrive now at the following relation between the internal forces P_1 and P_2 provided there is no slippage:

$$P_2 < P_1(\tan\alpha - \kappa)/(1 + \kappa\tan\alpha). \tag{7}$$

Once the slip occurs this relation turns into the following strict equation:

$$P_2 = P_1(\tan\alpha - \kappa)/(1 + \kappa\tan\alpha). \tag{8}$$

4

Considering P_2 in Eqn. 9 as the function of $\tan \alpha$ and taking the first derivative with respect to this argument we can arrive at a positive expression. Thus, to achieve an equilibrium of the four cylinders the side force P_2 must increase with increasing α. It means that if P_2 is constant, and P_1 exceeds a limiting value dictated by Eqn. 9 the system cannot stay in balance. In this case the system collapses and the angle α changes from its initial value to its upper limit of 60°.

The system collapse can be prevented provided that displacement boundary conditions are used. We can simulate the axial loading of the system increasing the vertical force P_1 and assuming that the system is limited in its expansion, so that the points S_1 and S_2 of the side cylinders (Fig. 4) do not suffer any displacements that can increase the system width. Thus, we arrive at the uniaxial deformation of the system. This computational experiment can be used to find the elastic modulus $M = \lambda + 2\mu$, where λ and μ denote the Lamé elastic constants of the cylinders material, and, thus, to estimate P-wave velocity.

To perform this experiment we applied at the beginning a certain confining pressure, and then gradually increased the vertical force P_1. Once slippage occured Eqn. 9 was used to calculate the force P_2 during the loading process. The angle α was changed to meet the conditions of zero displacements for the points S_1 and S_2.

Unloading the system we gradually decreased the vertical force P_1 checking the slippage condition (Eqn. 8). To find the force P_2 during the slippage, in the case when the tangential force T is directed to prevent the cylinder's upward motion, we used the following equation instead of Eqn. 9:

$$P_2 = P_1(\tan \alpha + \kappa)/(1 - \kappa \tan \alpha). \tag{9}$$

Eqns. 1 - 9 can be used to compute the displacements of the system during loading and unloading.

Numerical Examples

The computations were performed for the system of glass cylinders (E=62.27 GPa, ν=0.2466); the cylinder radius was 0.0375 mm. These parameters were used by Marion (1990) in his experiments conducted on glass beads. Friction coefficient, initial confining pressure (P_c) and initial geometry of the system were changed in our computational experiments to find the influence of these parameters on the elastic constants.

5

Four Cylinders System - Uniaxial Deformation

The stress-strain relationship for the four cylinders system during loading and unloading is presented in Fig. 5. In this case the initial parameters values were the following: $\alpha = 57^o$, $\kappa = 0.3$, $P_c = 0$. The initial value of angle α was about its upper limit of 60°. A vertical stress σ was calculated as a ratio of the vertical force P_1 to the width of the system. A displacement ε was found as the ratio of a vertical displacement and the initial vertical size of the system.

The stress-strain curve presented in Fig. 5 is similar to the theoretical curves obtained for the uniaxial strain loading of spheres in a face-centered cubic array, and the results of experiments performed on Ottawa sand (Stoll, 1989). The hysteresis effect appears due to the change of friction force direction at the contact area between adjacent cylinders. The initial pattern of the system deformation under loading condition is elastic. After sliding begins the system deforms plastically with the angle α increasing. In the beginning stage of unloading the upper cylinder is stuck between the side cylinders and the system deforms elastically. Ultimately, when sliding in the upward direction begins, the system deforms plastically.

The relationship between modulus M and vertical stress σ is presented in Fig. 6 for the case $\alpha = 57^o$, $\kappa = 0.3$ for two different values of the initial confining pressure: 0 and 10 MPa. The curve A corresponds to the curve in Fig. 5. Vertical lines connecting the bottom and top branches of the curve A represent the change of M when unloading is initiated at certain points of loading path and the system deforms elastically. These increased values of M are very close to those computed during the monotonous unloading of the four cylinders system (the top branch of the curve A). The difference between the bottom and the top branches of the curve A corresponds to a difference between "static" and "dynamic" elastic moduli of a grain material. In this example the ratio of the "dynamic" M to the "static" one has the order of 5.

The curve B in Fig. 6 corresponds to the case when the initial confining pressure is 10 MPa. The system becomes less compliant than in the case when $P_c = 0$. The last part of the unloading path (the top branch of the curve B) is close to an elastic pattern unlike the last part of the curve A when intensive plastic deformation occurs.

The computational uniaxial compression experiments were conducted on the four cylinders system for different angles α, friction coefficients κ and initial confining pressure P_c.

The loading-unloading curves for $\alpha = 57°$, $P_c = 0$ and $\kappa = 0.6$ and 1.2 are given in Fig. 7.

The increase of the friction coefficient κ results in increased "static" modulus (curve B, the bottom branch) and decreased "dynamic" modulus (curve B, the top branch). The latter effect is not as strong as the former one. The origin of observed difference between two unloading paths (curves A and B, the top branches) is the loading history.

The case of $\alpha = 45°$ and $P_c = 0$ is presented in Fig. 8. The values of friction coefficient were 0.6, 0.9, and 1.2. In the last case the system deformed elastically without a difference between loading and unloading patterns (curve C). Loading curves correspond to plastic deformation in the cases when $\kappa = 0.6$, and $\kappa = 0.9$. The "static" modulus M increases with increasing κ.

For $\alpha = 30°$ (the lower limit of this parameter) the system deforms elastically when the friction coefficient κ is as small as 0.6 (curve B, Fig. 9). The system deforms elastically even at $\kappa = 0.3$ provided that initial confining pressure is applied (curve C, Fig. 9).

If $\kappa = 0.3$ and $P_c = 0$ the system shows plastic behavior when loaded (the bottom branch of curve A, Fig. 9). The "dynamic" moduli calculated along the loading path are very close to those obtained from the elastic unloading path (the top branch of curve A, Fig. 9).

The above examples indicate the increasing stiffness of the system when angle α decreases. The difference between the "static" modulus (M_s) and the "dynamic" one (M_d) also decreases, so that the ratio M_d/M_s decreases from the order of 5 for $\alpha = 57°$ to the order of 1.5 for $\alpha = 30°$.

The change of angle α along the plastic deformation curves is very small and has the order of $0.5°$.

Four Cylinders System - Bulk Modulus

To calculate a bulk modulus K of the four cylinders system we apply equal vertical and horizontal forces: $P_1 = P_2$. Making use of this condition and Eqns. 6 we arrive at the following expression for the ratio of tangential to normal force at the contact zone:

$$\frac{T}{N} = \frac{\tan \alpha - 1}{\tan \alpha + 1}.$$

This relation gives the following range of T/N variation when angle α changes between $30°$ and $60°$: $-0.268 < T/N < 0.268$. The realistic values

of friction coefficient κ do not fall into this interval. Thus, the deformation of the system when equal vertical and horizontal forces are applied, follows an elastic pattern.

The relationships between the bulk modulus K and confining pressure P_c for different α are presented in Fig. 10. The values of K increase significantly when α decreases.

Reducing System's Stiffness

To reduce the stiffness of four cylinders system we assume that it is surrounded by rows of identical cylinders with zero displacements of the right and left external points (Fig. 11).

The results of uniaxial strain experiments for such a system are presented in Fig. 12. In this case the four cylinders system was surrounded by twelve cylinders on both sides. The values of angle α and friction coefficient were the following: $\alpha = 45°$, $\kappa = 0.6$.

The reduced stiffness of the system strongly affects the "static" modulus M (the loading curve, Fig. 12). The reduction of this parameter has the order of 5 for the example under consideration.

Discussion

Making use of an exact analytical solution for the plane deformation of an elastic cylinder and conducting computational experiments on the simple combinations of cylinders we observed the difference between "static" and "dynamic" elastic moduli for grain material. This approach allows the employment of more complicated and realistic combinations of cylinders for modeling granular material.

The simplest approach to model a granular aggregate is to combine four-grain units with different friction coefficients and initial configurations in rows and columns. The distribution of mentioned parameters will depend on actual properties of unconsolidated rocks. The numerical experiments conducted on such models result in relationships similar to those presented in Figs. 5 - 10. The values of elastic moduli for the aggregates are equal to weighted averages of these parameters for single four-grain units.

Conclusions

Considering the system of four elastic cylinders interacting with friction we discover the difference between "static" and "dynamic" elastic moduli when

8

slippage occurs.

The "static" modulus of the system depends strongly on initial configuration, friction coefficient and confining pressure. The "dynamic" modulus depends mainly on initial configuration and confining pressure.

The system's stiffness can be significantly reduced due to mild boundary conditions (four cylinders surrounded by rows of cylinders).

The elastic properties of aggregates of four-grain units having different initial configurations and friction coefficients are similar to those of single units. The values of elastic moduli are equal to weighted averages of these moduli for four-grain units.

REFERENCES

1. Gassman, F., 1951, Elastic waves through a packing of spheres: Geophysics, 16, 673-685.

2. Deresiewicz, H., 1958, Stress-strain relations for a simple model of a granular medium: J. Appl. Mech., 25, 402-405.

3. Digby, P.J., 1981, The effective elastic moduli of porous granular rocks: J. Appl. Mech., 48, 803-808.

4. Duffy, J., and Mindlin, R.D., 1957, Stress-strain relations and vibrations of a granular medium: J. Appl. Mech., 24, 585-593.

5. Johnson, K.L., 1984, Contact mechanics, Cambridge University Press.

6. Marion, D.P., 1990, Acoustical, mechanical, and transport properties of sediments and granular materials: Ph.D. dissertation, Stanford University.

7. Mindlin, R.D., 1954, Mechanics of granular media: Proc. 2nd U.S. Nat. Cong. Appl. Mech., ASME, New York, 13-20.

8. Novozhilov, V.V., 1961, Theory of elasticity, Pergamon Press.

9. Stoll, R.D., 1989, Sediment Acoustics, Springer-Verlag.

10. Walton, K., 1975, The effective elastic moduli of model sediments: Geophys. J.R. Astro. Soc., 43, 293-306.

11. Walton, K., 1987, The effective elastic moduli of a random packing of spheres: J. Mech. Phys. Solids, 35, 2, 213-226.

12. White, J.E., 1965, Seismic waves: radiation, transmission and attenuation, McGraw-Hill, N.Y.
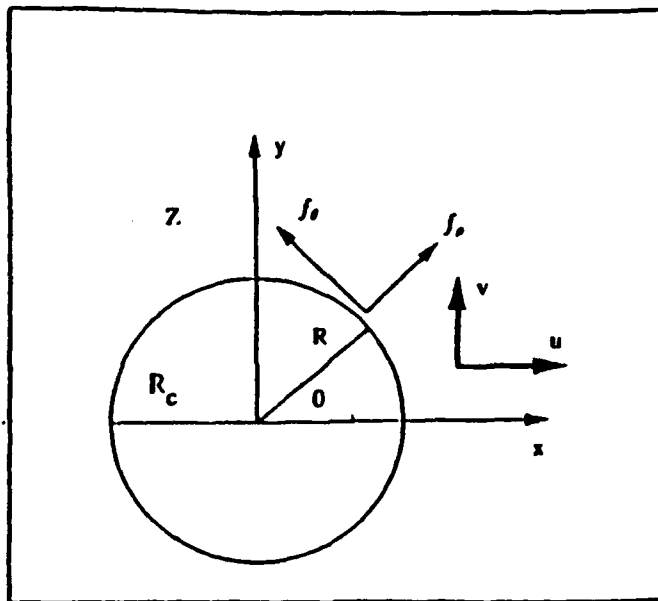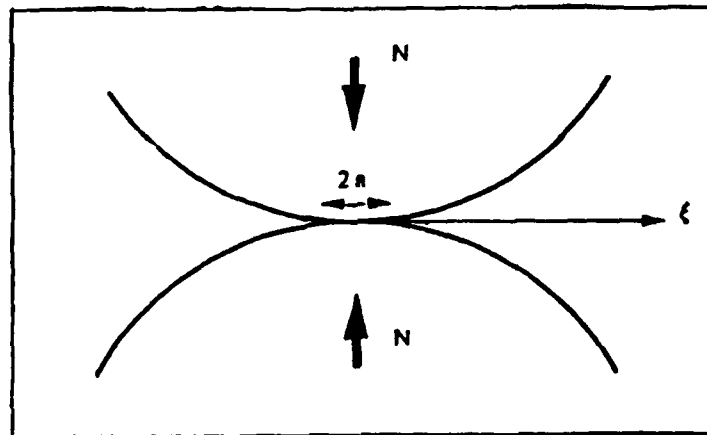
Figure 1 : A circular cylinder in the complex plane z.
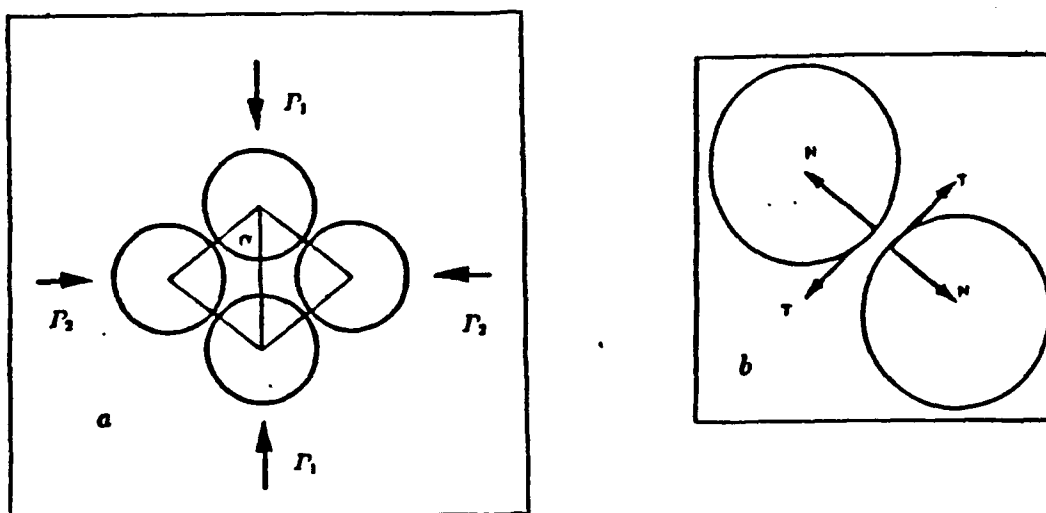

Figure 2 : The contact zone of two cylinders.

Figure 3 : A. Four cylinders combination. B. Normal and tangential reactive forces between two cylinders.
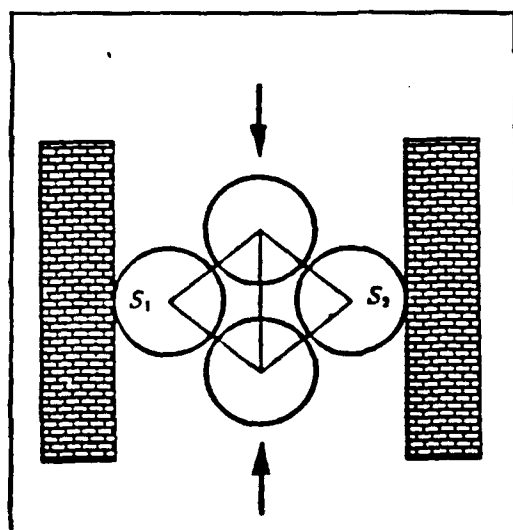

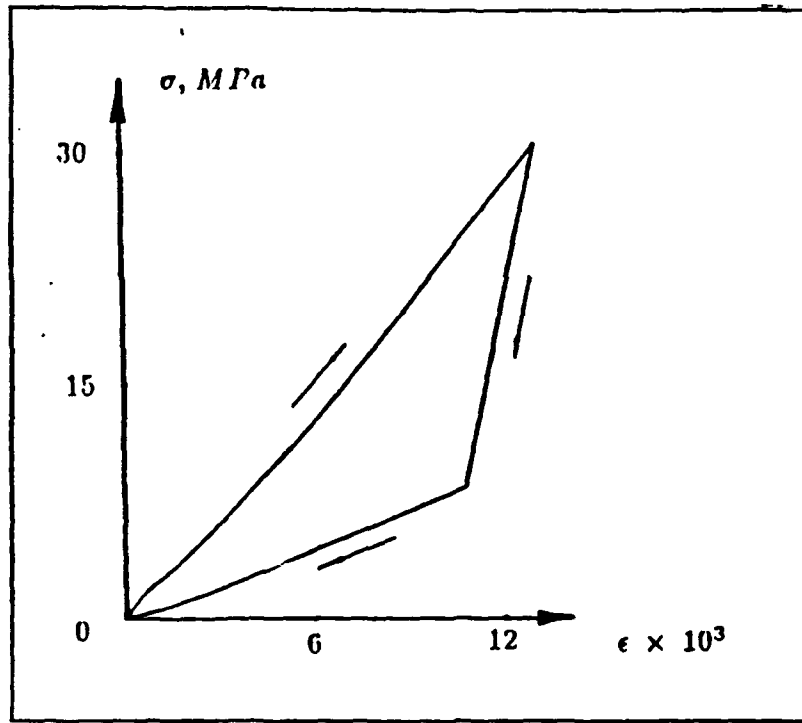**Figure 4** : Four cylinders system - uniaxial deformation.

Figure 5 : Stress-strain relationship for the uniaxial deformation of four cylinder system; $\alpha = 1$, $\kappa = 0.3$, $P_c = 0$.
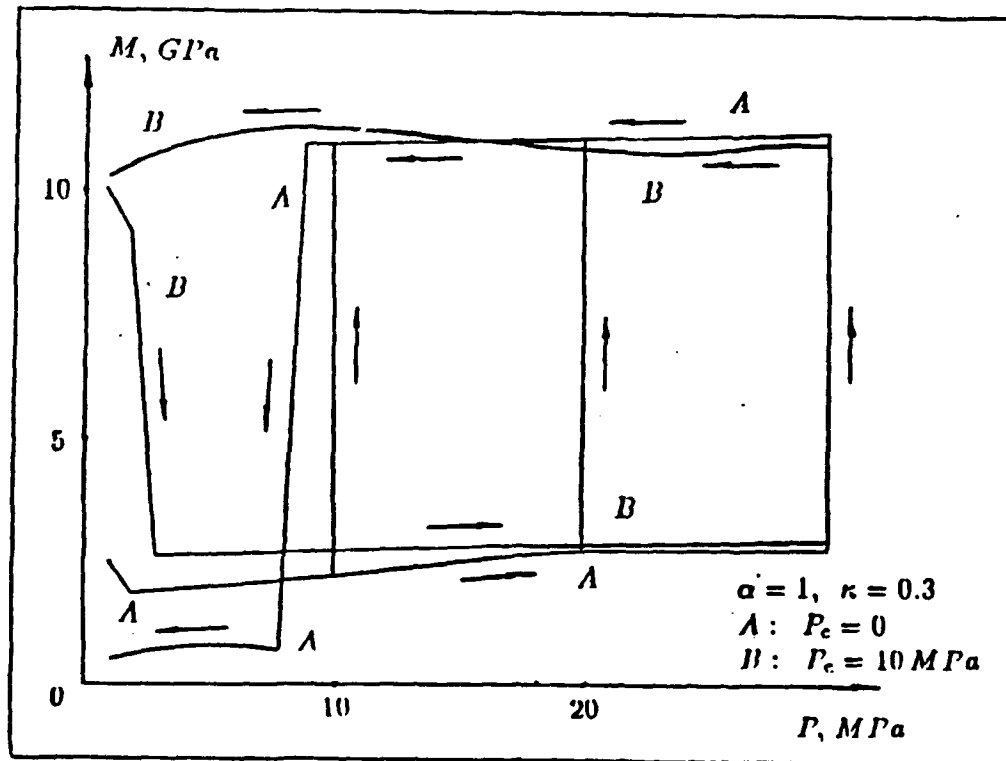

Figure 6: $M - P$ relationship for the four cylinders system; $\alpha = 57°$, $\kappa = 0.3$, $P_c = 0$ and $10\,MPa$.
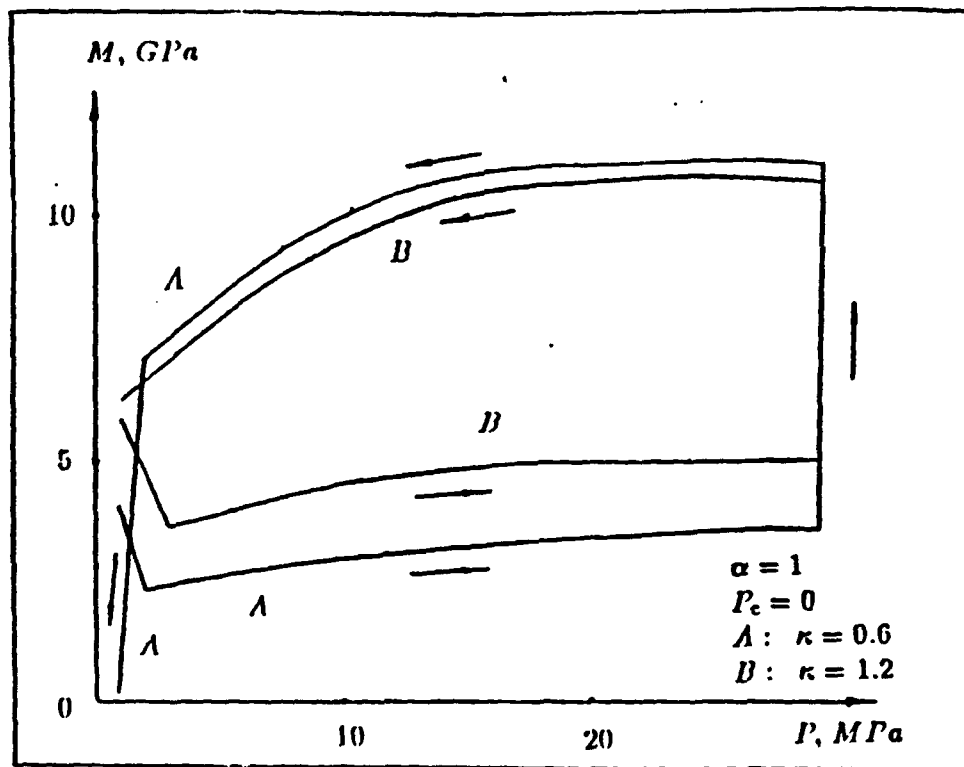
Figure 7 : $M - P$ relationship for the four cylinders system; $\alpha = 57°$, $P_c = 0$, $\kappa = 0.6$ and 1.2.
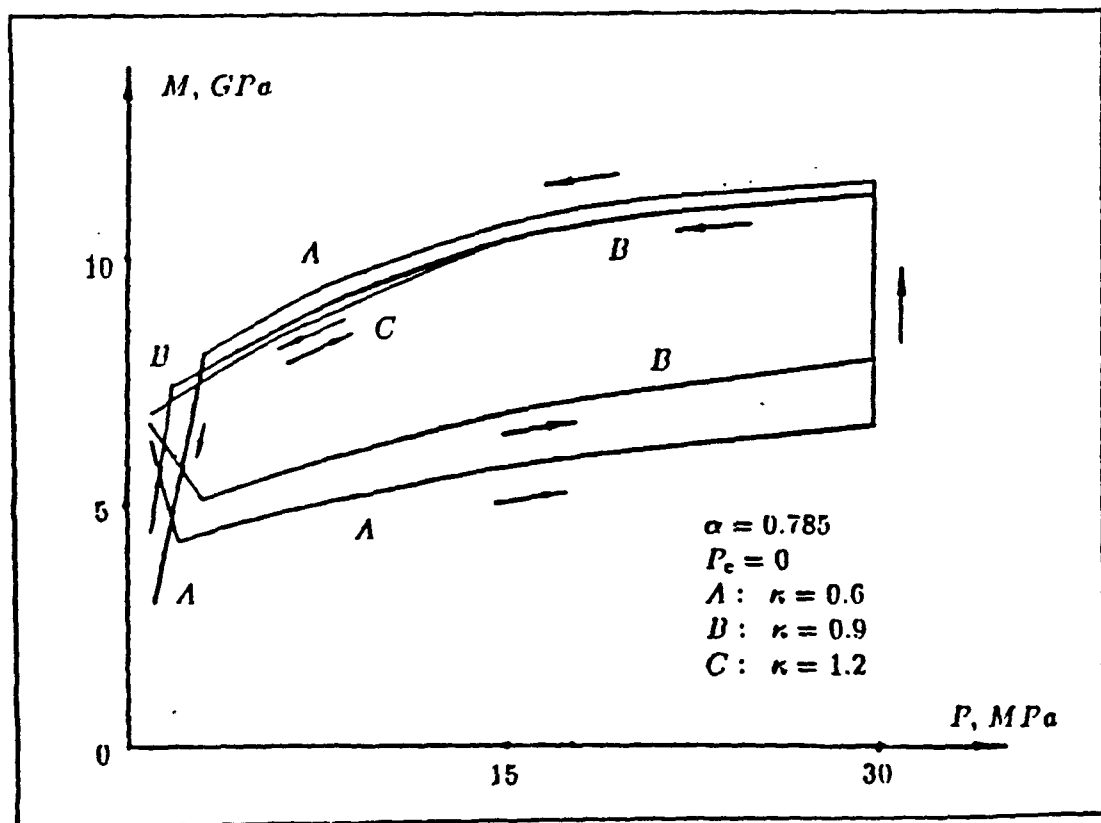

Figure 8 : $M - P$ relationship for the four cylinders system; $\alpha = 45°$, $P_c = 0$, $\kappa = 0.6$, 0.9, and 1.2.
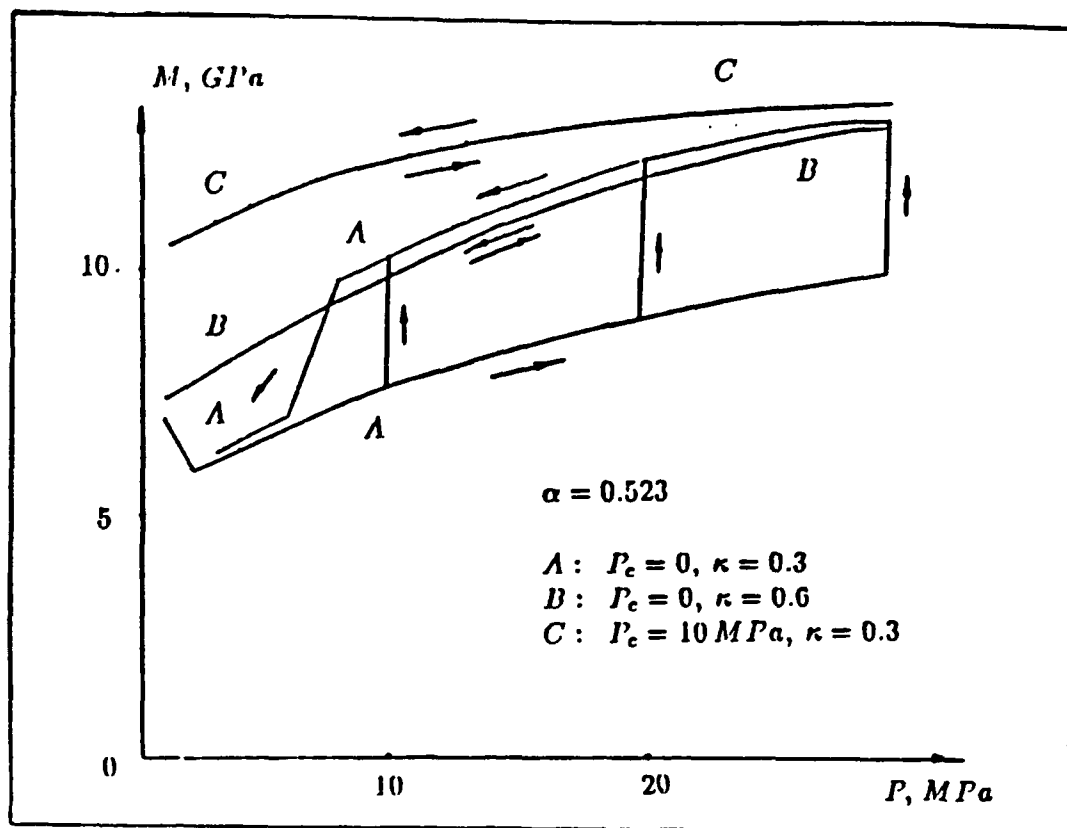
Figure 9 : $M - P$ relationship for the four cylinders system; $\alpha = 30°$, $P_c = 0$, and 10 MPa, $\kappa = 0.3$, and 0.6.
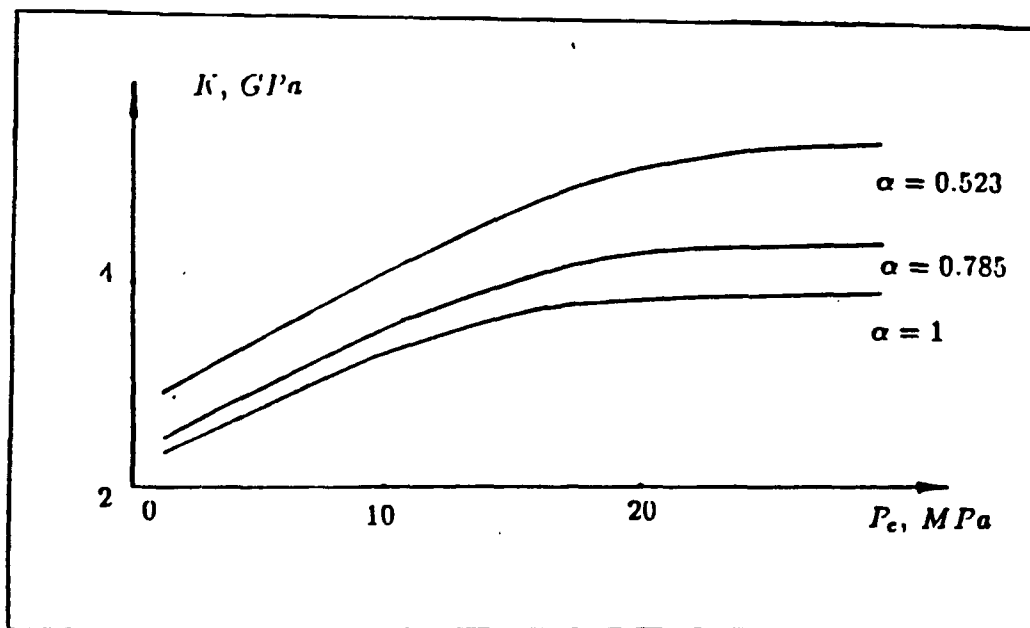

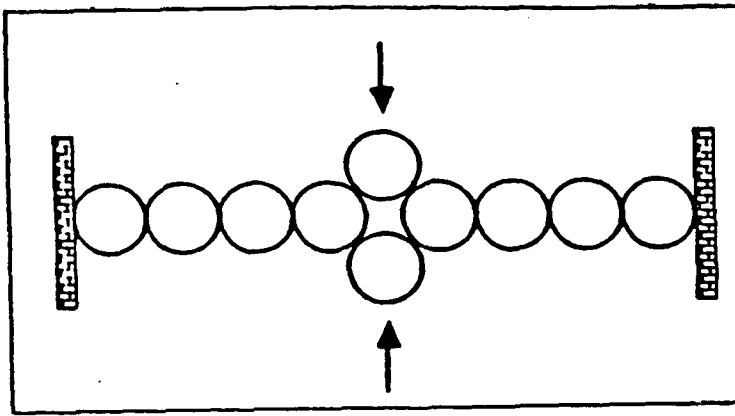**Figure 10** : K versus P_c for $\alpha=30°$, $45°$, and $60°$.

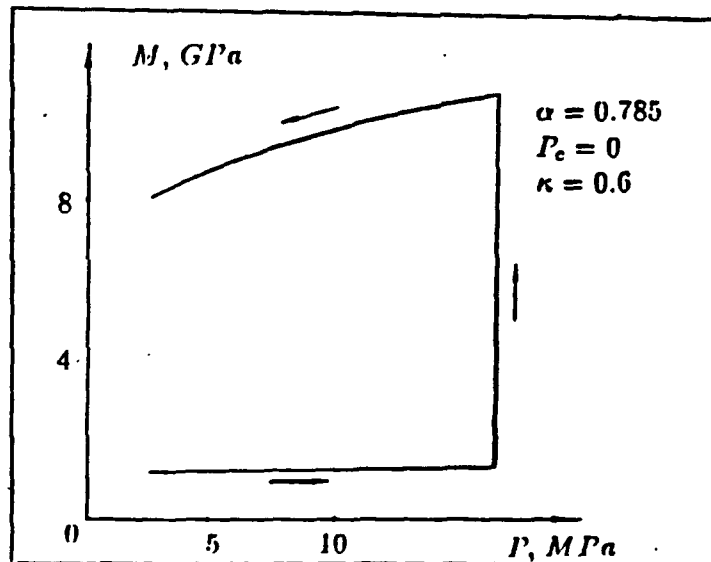**Figure 11 :** The system of reduced stiffness.

Figure 12 : $M - P$ relationship for the system of reduced stiffness; four cylinders system is surrounded by 12 cylinders on both sides; $\alpha = 45^\circ$, $\kappa = 0.6$.

The Mechanics of Hollow Grains

Abstract

We develop a theory of the two-dimensional deformation of hollow grains under external loading, modeling them as cylindrical shells of a closed cross-section. This theory allows us to describe the deformation of arbitrarily-shaped grains with walls of varying thickness, and external and internal fractures. Fractures dramatically reduce the stiffness of the grains and may result in the collapse and compaction of hollow grains under lithostatic pressure. Calculating the normal and shear stiffness of hollow grains, one will be able to determine effective elastic properties of their aggregate using the expressions developed for a random packing of spheres. The theory presented in this paper can be directly applied to estimating the acoustical and mechanical properties of basaltic pillows and pelagic sediments.

Introduction

The acoustic and mechanical characteristics of oceanic crust and seabottom sediments may be strongly affected by the properties of individual grains that compose the material. Almost all theoretical models for the deformation of a granular material treat an individual grain as an elastic element without voids, typically as a disk (2D) or a sphere (3D). Recently, Bruno and Nelson (1990) examined the effect of intergranular microfractures on the inelastic behavior of sedimentary rock. The deformation of the aggregate of arbitrarily-shaped grains can, in principle, be modeled using the numerical simulation of the deformation of an individual grain combined with a numerical model for granular assemblies (Cundall and Strack, 1979).

However, there are at least two cases where grains with interior voids have to be considered: (1) basaltic pillows that are present in the oceanic crust, and (2) pelagic sediments formed by hollow shells. In this paper we concentrate on the theoretical description of the deformation of a hollow

1

arbitrarily-shaped grain under given loading. We model a grain as a cylindrical shell of arbitrarily-shaped middle surface and varying thickness. This approach allows us to introduce external and internal cracks in the walls of the grain as well as to examine the effect of differently-shaped internal holes. The problem is reduced to a system of ordinary differential equations that requires numerical solution. We show how the shape and fracturing affect the stiffness of grains.

This is a two-dimensional theoretical approach, but it can quantitatively predict the characteristics of elongated basaltic pillows, and can give qualitative estimates of behavior of topologically complicated pelagic sediments.

Deformation of Cylindrical Shells

In this section we derive a general theory for the 2-D deformation of cylindrical shells using assumptions common for the theory of thin shells. Typically, a shell is considered to be thin if the ratio of its thickness $2h$ to the radius of curvature of its middle surface R is less than .05. This condition guarantees the accuracy of results within a 5% range. However, the theory of thin shells can be also applied (with decreased accuracy) for thick shells with the ratio $2h/R$ having the magnitude up to 1/3 (Grigoluk and Kabanov, 1978). Thus the theory of deformation of hollow grains based on the theory of shells is accurate enough to quantitatively estimate the acoustical and mechanical properties of basaltic pillows and pelagic sediments.

Displacements and Forces in Cylindrical Shells

To examine the 2-D deformation of an infinitely long cylindrical shell (Fig. 1A), we introduce a local cylindrical coordinate system (θ, r) in the normal cross-section of the shell (Fig. 1B). The center of the (θ, r) coordinate system is placed in the local center of curvature of the middle surface of the shell. We also introduce a local rectangular coordinate system (x, z) with the origin in the middle surface of the shell, the x axis tangent to this surface, and the z axis directed along the radius of curvature. These two coordinate systems are related to each other as:

$$x = R\theta; \quad z = r - R. \tag{1}$$

The displacements of the shell are $\tilde{u}(x, z)$ in the x direction and $\tilde{w}(x, z)$ in the z direction. We assume the following form of functional dependence

2

of these displacements on the x and y arguments:

$$\tilde{u}(x,z) = u^\circ(x) + z\phi(x); \quad \tilde{w}(x,z) = w^\circ(x). \tag{2}$$

This assumption implies that a straight fiber initially perpendicular to the middle surface keeps its straight shape after deformation and tilts at angle ϕ to its initial direction (Fig. 2A), and the thickness of the shell does not change.

We examine the case of a plane deformation of the shell: $e_{yy} = 0$, where e_{yy} is a normal deformation in the y direction perpendicular to the plane of deformation. This condition and Hook's law yield:

$$\frac{\sigma_{yy}}{E} - \nu\frac{\sigma_{rr} + \sigma_{\theta\theta}}{E} = 0, \tag{3}$$

where E is Young's modulus; ν is Poisson's ratio; σ_{yy}, σ_{rr} and $\sigma_{\theta\theta}$ are components of a stress tensor in the shell.

Commonly, in the theory of plates and shells it is assumed that the normal stress in the direction perpendicular to the middle surface is small compared to the other normal stresses (Timoshenko and Woinowsky-Krieger, 1959): $\sigma_{rr} + \sigma_{\theta\theta} \approx \sigma_{\theta\theta}$. This assumption and (3) yield:

$$\sigma_{yy} = \nu\sigma_{\theta\theta}. \tag{4}$$

Using (4) and Hook's law we arrive at the following relations between the components of the stress and deformation tensors:

$$\sigma_{\theta\theta} = \frac{E}{1 - \nu^2}e_{\theta\theta}; \quad \sigma_{r\theta} = \frac{E}{1 + \nu}e_{r\theta}. \tag{5}$$

The components of the deformation tensor can be related to the displacements $\tilde{u}$ and $\tilde{w}$, and functions u°, w° and ϕ in the (θ, r) cylindrical coordinate system as:

$$e_{\theta\theta} = \frac{1}{r}(\frac{\partial \tilde{u}}{\partial \theta} + \tilde{w}) = \frac{1}{r}(\frac{\partial u^\circ}{\partial \theta} + z\frac{\partial \phi}{\partial \theta} + w^\circ),$$

$$2e_{r\theta} = \frac{1}{r}\frac{\partial \tilde{w}}{\partial \theta} + \frac{\partial \tilde{u}}{\partial \theta} - \frac{\tilde{u}}{r} = \frac{1}{r}\frac{\partial w^\circ}{\partial \theta} + \phi - \frac{u^\circ}{r} - \frac{\phi z}{r}.$$

Using (3) and assuming that $r \approx R$ in the shell, we transform these equations to:

$$e_{\theta\theta} = \frac{\partial u^\circ}{\partial x} + z\frac{\partial \phi}{\partial x} + \frac{w^\circ}{R}; \quad 2e_{r\theta} = \frac{\partial w^\circ}{\partial x} + \phi - \frac{u^\circ}{R} - \frac{\phi z}{R}. \tag{6}$$

3

We introduce integral normal N and shear Q forces in the shell, and bending moment M (Fig. 2B) created by normal stresses as:

$$N = \int_{-h}^{h} \sigma_{\theta\theta} dz; \quad Q = \int_{-h}^{h} \sigma_{r\theta} dz; \quad M = \int_{-h}^{h} \sigma_{\theta\theta} z dz. \tag{7}$$

Using these definitions and relations (5) and (6), we express the integral forces and the bending moment through functions u^o, w^o and ϕ:

$$Q = \frac{Eh}{1+\nu}\left(\frac{\partial w^o}{\partial x}+\phi-\frac{u^o}{R}\right); \quad N = \frac{2Eh}{1-\nu^2}\left(\frac{\partial u^o}{\partial x}+\frac{w^o}{R}\right); \quad M = \frac{2Eh^3}{3(1-\nu^2)}\frac{\partial \phi}{\partial x}. \tag{8}$$

It is important to mention that the x coordinate can be continuously counted along the middle surface of the shell by varying x between 0 and L, where L is the shell's perimeter. This approach will not change the above-derived formulas as they include only the differential dx. Parameters R and h have to be considered as functions of x.

Equations of Shell's Deformation

The equations for the deformation of the shell under external forces will be derived from the equations of static elasticity:

$$\frac{\partial(r\sigma_{rr})}{\partial r} + \frac{\partial \sigma_{r\theta}}{\partial \theta} - \sigma_{\theta\theta} = 0; \tag{9}$$

$$\frac{\partial(r\sigma_{r\theta})}{\partial r} + \frac{\partial \sigma_{\theta\theta}}{\partial \theta} + \sigma_{r\theta} = 0. \tag{10}$$

Integrating (9) from $-h$ to h in the z direction and using (1) and (7) we have:

$$R(\sigma_{rr}|_h - \sigma_{rr}|_{-h}) + R\frac{\partial Q}{\partial x} - N = 0,$$

or

$$\frac{\partial Q}{\partial x} - \frac{N}{R(x)} = -F(x), \tag{11}$$

where $F(x) = \sigma_{rr}|_h - \sigma_{rr}|_{-h}$ is the difference between external and internal normal tractions acting on the shell.

Integrating (10) from $-h$ to h in the z direction and using (1) and (7) we have:

$$R(\sigma_{r\theta}|_h - \sigma_{r\theta}|_{-h}) + R\frac{\partial N}{\partial x} + Q = 0,$$

or

$$\frac{\partial N}{\partial x} + \frac{Q}{R(x)} = -T(x), \tag{12}$$

where $T(x) = \sigma_{r\theta}|_h - \sigma_{r\theta}|_{-h}$ is the difference between external and internal shear tractions acting on the shell.

Multiplying (10) by z and integrating from $-h$ to h in the z direction and using (1) and (7) we have:

$$\int_{-h}^{h}(r\frac{\partial\sigma_{r\theta}}{\partial r} + \frac{\partial\sigma_{\theta\theta}}{\partial\theta} + 2\sigma_{r\theta})z\,dz = \frac{\partial M}{\partial\theta} + \int_{-h}^{h}(R+z)z\frac{\partial\sigma_{r\theta}}{\partial z}dz.$$

The last integral in this equation is:

$$(R+z)z\sigma_{r\theta}|_{-h}^{h} - \int_{-h}^{h}(R+2z)\sigma_{r\theta}dz \approx -RQ + (R+h)h\sigma_{r\theta}|_h + (R-h)h\sigma_{r\theta}|_{-h}.$$

Using these formulas we arrive at the equation that includes the bending moment M:

$$\frac{\partial M}{\partial x} - Q = -S(x), \tag{13}$$

where $S(x) = (1+h/R)h\sigma_{r\theta}|_h + (1-h/R)h\sigma_{r\theta}|_{-h}$ is the ratio of the moment due to external and internal shear tractions to the local radius of curvature.

Substituting (8) into equations (11)-(13) we arrive at the following equations in terms of displacements:

$$w_{xx}^o + w_x^o\frac{h_x}{h} - u^o\frac{3-\nu}{R(1-\nu)} + \phi_x - \frac{2w^o}{(1-\nu)R^2} + \frac{u^o}{R}(\frac{R_x}{R} - \frac{h_x}{h}) + \phi\frac{h_x}{h} = -\frac{F(1+\nu)}{Eh};$$

$$u_{xx}^o + w^o\frac{3-\nu}{2R} + u_x^o\frac{h_x}{h} - \frac{w^o}{R}(\frac{R_x}{R} - \frac{h_x}{h}) - \frac{u^o(1-\nu)}{2R^2} + \tag{14}$$

$$\frac{\phi(1-\nu)}{2R} = -\frac{T(1-\nu^2)}{2Eh};$$

$$h\phi_{xx} - w_x^o\frac{3(1-\nu)}{2h} + 3h_x\phi_x + u^o\frac{3(1-\nu)}{2Rh} - \phi\frac{3(1-\nu)}{2h} = -\frac{3}{2}\frac{S(1-\nu^2)}{Eh^2}.$$

Subscripts "x" and "xx" in these equations indicate partial derivatives from functions u^o, w^o and ϕ.

We introduce normalized variables u, w and ξ as:

$$w^o = Lw;\ u^o = Lu;\ x = L\xi.$$

5

Substituting these formulas into (14) we have:

$$w_{\xi\xi} + a(\xi)w_\xi - u_\xi\kappa(\xi)\frac{3-\nu}{1-\nu} + \phi_\xi - \frac{2\kappa^2(\xi)}{1-\nu}w + u\kappa(\xi)b(\xi) + \phi a(\xi) = -f(\xi);$$

$$u_{\xi\xi} + a(\xi)u_\xi + w_\xi\kappa(\xi)\frac{3-\nu}{2} - w\kappa(\xi)b(\xi) - \frac{\kappa^2(\xi)(1-\nu)}{2}u+ \quad (15)$$

$$\phi\frac{\kappa(\xi)(1-\nu)}{2} = -t(\xi);$$

$$\phi_{\xi\xi} + 3a(\xi)\phi_\xi - w_\xi\frac{3(1-\nu)}{2\epsilon^2(\xi)} + \frac{3(1-\nu)}{2\epsilon^2(\xi)}\kappa(\xi)u - \frac{3(1-\nu)}{2\epsilon^2(\xi)}\phi = -s(\xi),$$

where

$$a(\xi) = \frac{d(\ln h)}{d\xi}; \quad b(\xi) = \frac{d}{d\xi}(\ln\frac{R}{h}); \quad \kappa(\xi) = \frac{L}{R(\xi)}; \quad \epsilon(\xi) = \frac{h(\xi)}{L};$$

$$f(\xi) = \frac{F(\xi)(1+\nu)L}{Eh(\xi)}; t(\xi) = \frac{T(\xi)(1-\nu^2)L}{2Eh(\xi)}; s(\xi) = \frac{3}{2}\frac{S(\xi)(1-\nu^2)L^2}{Eh^3(\xi)}.$$

This system of ordinary differential equations of the second order can be solved with the following boundary conditions:

$$w(0) = u(0) = \phi(0) = w(1) = u(1) = \phi(1) = 0. \quad (16)$$

Conditions (16) express the requirement of continuity of displacements along a shell of a closed cross-section. In addition, we fix the displacements at the origin of the x coordinate system setting them equal to zero. This is a usual condition of fixing a point in an elastic body in order to predefine its rigid translation.

Equations (15) with boundary conditions (16) allow us to find the displacement of the shell in the x coordinate system. The x coordinate is counted along the cross-section of the middle surface of the shell; the direction of the displacement depends on the local geometry of the middle surface as w is perpendicular to the middle surface and u is tangent to it.

The Shape of the Shell

In order to relate the displacements of the shell in the x coordinate system to its geometrical configuration, we introduce a reference rectangular coordinate system (x_0, y_0) in the plane of deformation (Fig. 3). The geometry of

6

the middle surface of the shell can be given in the (x_0, y_0) coordinate system in a parametric form:

$$x_0 = x_0(\tau), \quad y_0 = y_0(\tau), \tag{17}$$

where parameter τ spans an interval $0 < \tau < T$. This parameter can be chosen, for example, as a central angle α changing between 0 and 2π.

The length L and the local curvature radius $R(\tau)$ can be found as:

$$L = \int_0^T \sqrt{\dot{x}_0^2 + \dot{y}_0^2}\, d\tau; \quad R(\tau) = \frac{(\dot{x}_0^2 + \dot{y}_0^2)^{3/2}}{\dot{x}_0 \ddot{y}_0 - \dot{y}_0 \ddot{x}_0}. \tag{18}$$

The local coordinate x is related to the parametric equations (17) as:

$$x = \int_c^\tau \sqrt{\dot{x}_0^2 + \dot{y}_0^2}\, d\tau. \tag{19}$$

Normalized coordinate $\xi = x/L$ is calculated using (18) and (19).

The process of calculating the deformation of a shell under a given loading includes the numerical solution of equations (15) with boundary conditions (16), and consequent calculation of the shape of the shell after deformation in a reference coordinate system (x_0, y_0). The latter procedure has simple numerical implementation based on the fact that displacement u is tangent to the middle surface of the shell and w is normal to this surface.

Numerical Examples

In this section we give two numerical examples considering: (1) the deformation of a circular hollow grain with and without cracks; and (2) the deformation of an elliptical hollow grain. In both cases grains deform due to compression along the vertical axis. The magnitudes of acting forces are highly exaggerated in order to make the deformation visible in the plots presented below. In reality, the forces of such magnitudes will result in plastic yield of grains.

Circular Grain

We examine the deformation of a circular hollow grain with and without radial cracks (Fig. 4) due to compression along the vertical direction. Two radial fractures dramatically reduce the stiffness of the grain (Fig. 5). This effect may be used to explain the existence of the shallow low velocity zones

7

in pillow basalts. The closure of cracks due to confining pressure increasing with depth will result in a sharp stiffness, and seismic velocity increase.

Normal (w) and tangential (u) displacements along the surface of the circular hollow grains are plotted in Fig. 6. Displacements in the fractured grain (curves **a** and **c**) are significantly larger than in the grain without cracks (curves **b** and **d**).

Elliptical Grain

Computations show that the stiffness of an unfractured elliptical hollow grain (Fig. 7) in the vertical direction is close to the stiffness of an unfractured circular grain. However the stiffness of the elliptical grain in the horizontal direction is more than twice its vertical stiffness. The deformed shape of the vertically loaded elliptical grain (a) is compared to its initial shape (b) in Fig. 8.

Conclusions

We presented a theory of the two-dimensional deformation of hollow grains under external loading, modeling them as cylindrical shells of a closed cross-section. This theory allows us to describe the deformation of arbitrarily-shaped grains with walls of varying thickness, and external and internal fractures. Fractures dramatically reduce the stiffness of the grains. This fact may be used to explain the existence of the shallow low velocity zones in pillow basalts. The closure of cracks due to confining pressure increasing with depth will result in a sharp stiffness, and seismic velocity increase. The theory presented in this paper can be directly applied to estimating the acoustical and mechanical properties of basaltic pillows and pelagic sediments.

References

1. Bruno, M.S. and Nelson, R.B., "Microstructural Analysis of the Inelastic Behavior of Sedimentary Rock," 1990, Chevron Oil Field Research Company, La Habra.

2. Cundall P.A. and Strack O.D., "A Discrete Numerical Model for Granular Assemblies," 1979, Geotechnique, 29, 1.

3. Grigoluk, E.I. and Kabanov, V.V., "The Stability of Shells," 1978, "Science," Moscow.

8

4. Timoshenko, S. and Woinowsky-Krieger, S., "Theory of Plates and Shells," 1959, McGRAW-HILL.
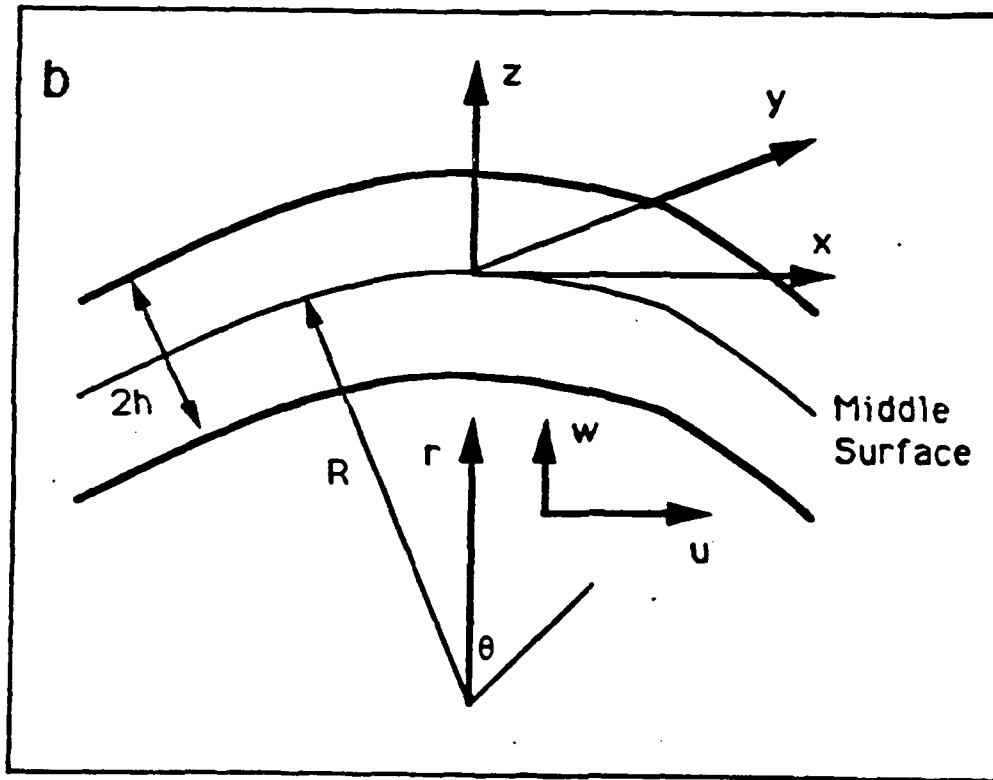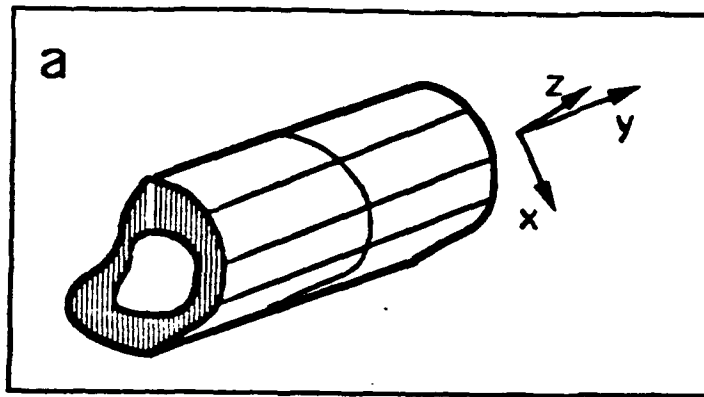
Figure 1: A. Arbitrarily-shaped hollow cylindrical shell and a local rect-angular coordinate system (x, y, z). B. local coordinate systems (θ, r) and (x, z).
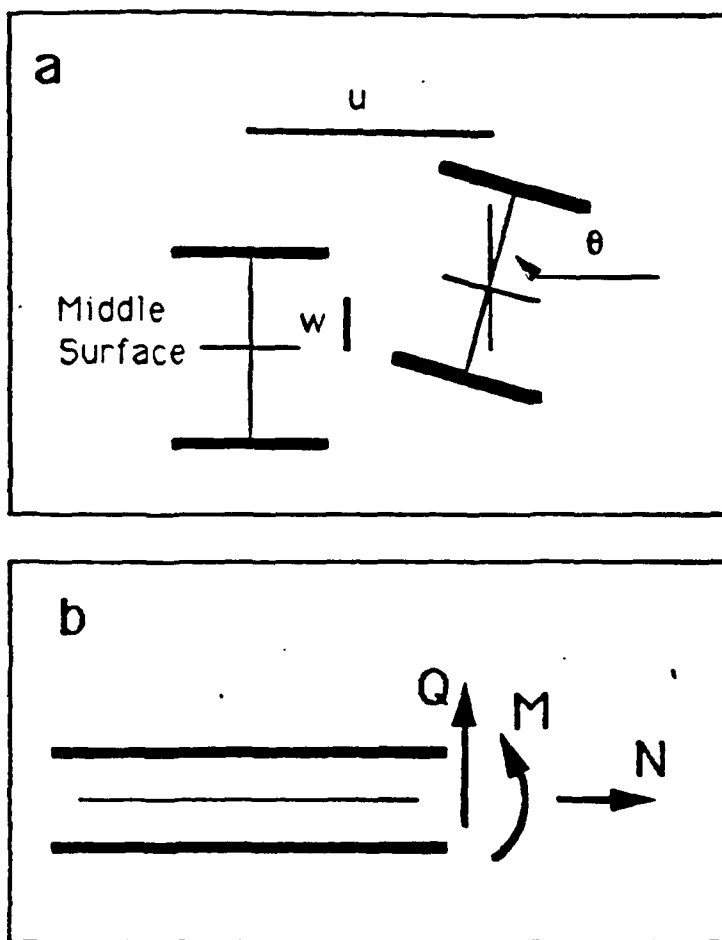
Figure 2: A. The assumed pattern of the shell's deformation. B. forces and moments in the shell.
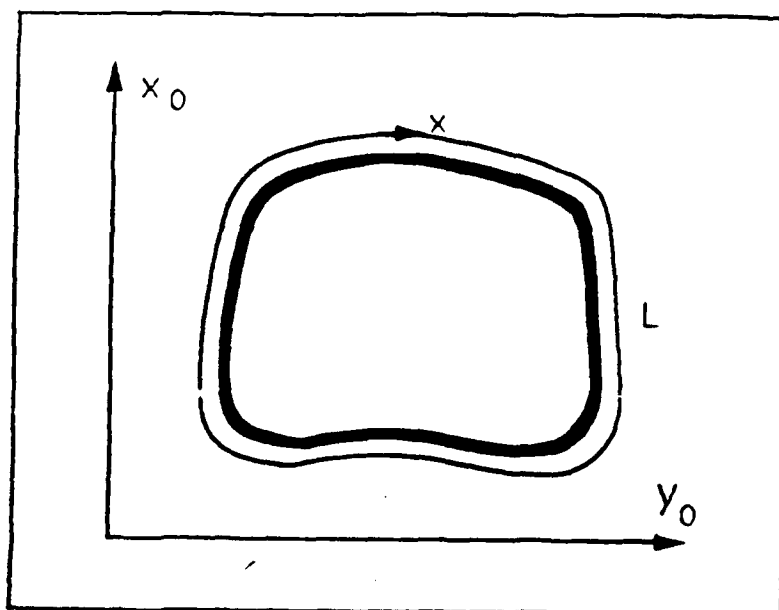

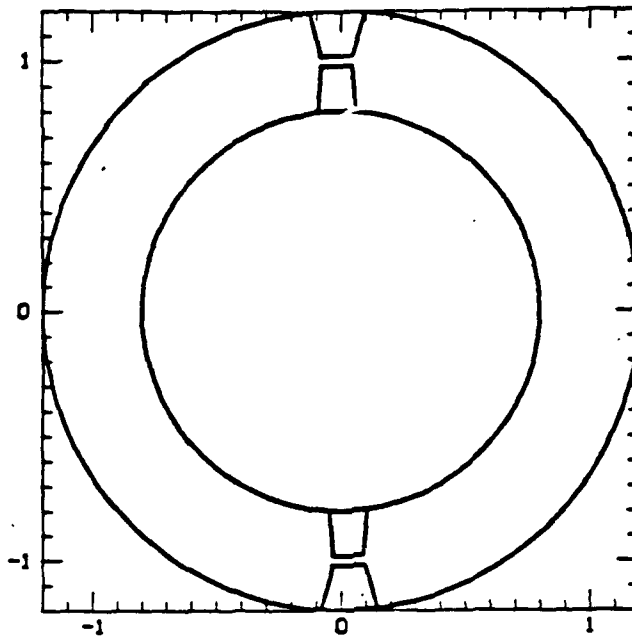**Figure 3:** The shell in a reference rectangular coordinate system (x_0, y_0).

Figure 4: Circular hollow grain with two radial cracks.
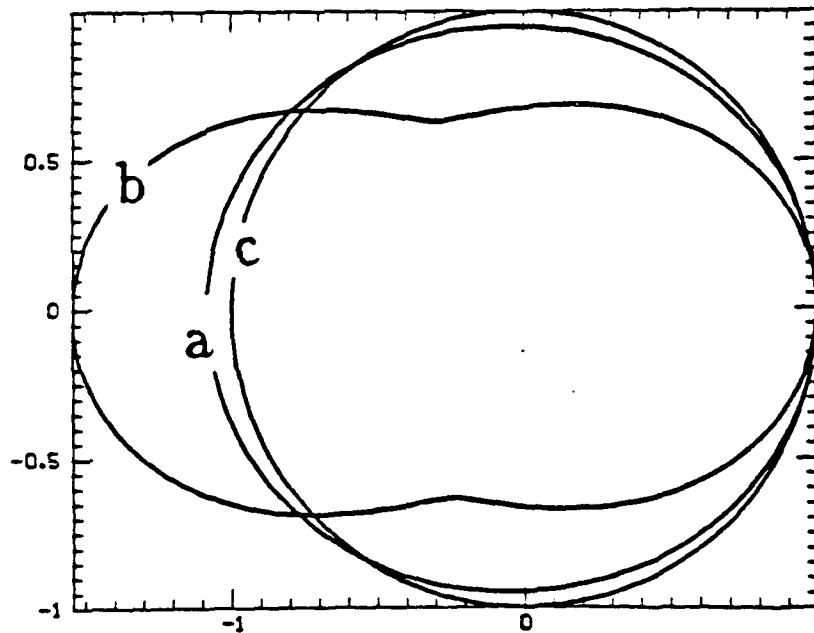
Figure 5: The deformed shapes of circular hollow grains without cracks (a) and with two cracks (b) due to vertical compression. Curve c represents the initial circular shape.

Figure 6: Displacements along the surface of the circular hollow grains: displacement w in the fractured (a) and unfractured (b) grain; displacement u in the fractured (c) and unfractured (d) grain.

Figure 7: Elliptical hollow grain.

Figure 8: The deformed shape of the elliptical hollow grain (a) compared to its initial shape (b).

Pillow Basalts Compaction due to Grain Collapse

Abstract

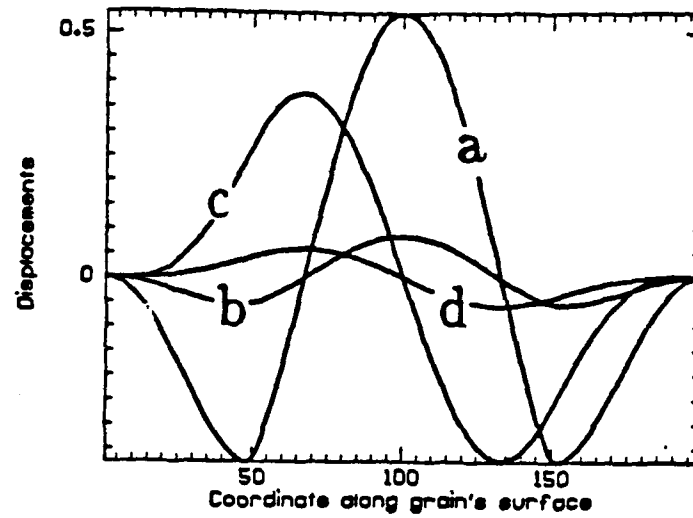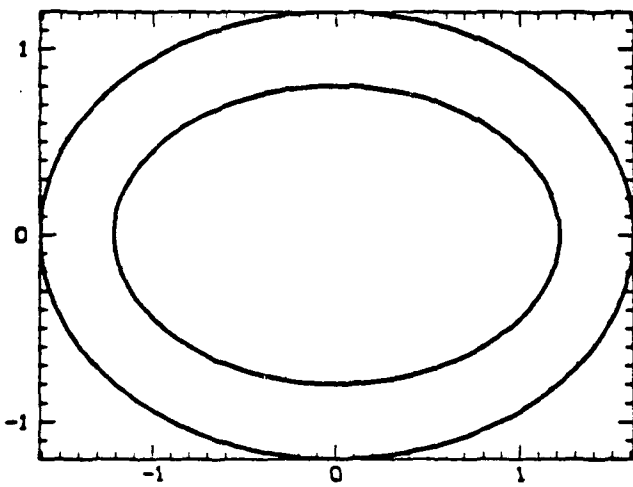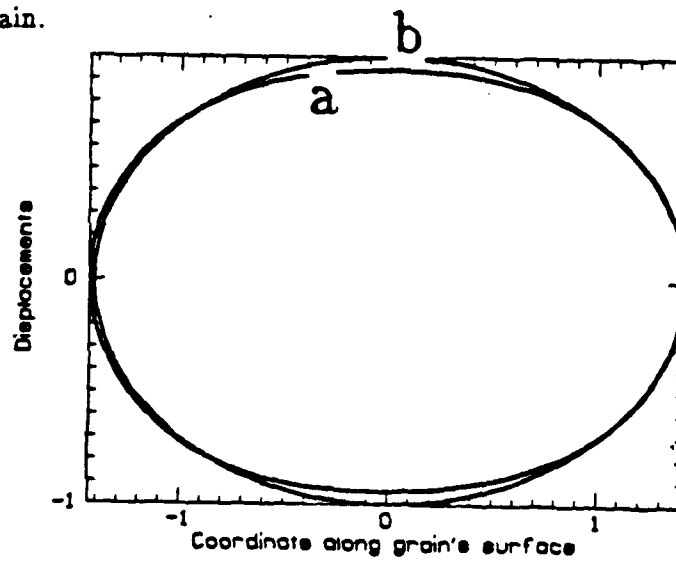A possible mode of compaction of pillow basalts and pelagic sediments (both formed by hollow grains) is by the collapsing of the grains due to increasing confining pressure. We derive simple criteria for the collapse of 2-D thick-walled, and thin-walled circular grains subject to external and internal pressure.

Introduction

Assuming that the compaction of pillow basalts and pelagic sediments may occur as the collapse of hollow grains that form those rocks, we derive simple criteria for the compaction due to increasing confining pressure.

We examine the deformation of a 2-D thick-walled cylinder due to internal and external pressure. To find the criterion of the collapse of such a cylinder we employ the solution for the elasto-plastic deformation of a thick-walled tube. The collapse occurs if the entire cylinder is in the mode of plastic deformation. In this solution we use the Mises plastic criterion.

In addition we give simple formulas for the collapse of a thin-walled cylindrical tube (shell).

These formulas can be used for estimating the depth of transition from low-velocity to high-velocity zones in the ocean bottom rocks. This transition is presumably connected with the compaction of hollow grains.

Deformation and Collapse of a Thick-Walled Shell

In this section we follow the solution for the elasto-plastic deformation of a thick-walled tube (e.g. Godfrey, 1969).

The equation of balance of a thick-walled tube subjected to the internal pressure P_1 and external pressure P_2 (Fig. 1) in the cylindrical coordinate

system (r, θ) is:

$$\frac{d\sigma_{rr}}{dr} = \frac{\sigma_{\theta\theta} - \sigma_{rr}}{r}, \tag{1}$$

where $\sigma_{\theta\theta}$ and σ_{rr} are normal stresses. Equation (1) holds both for plastic and for elastic zones of the tube.

The solution of (1) with the boundary conditions $\sigma_{rr} = P_1$ at $r = a$ and $\sigma_{rr} = P_2$ at $r = b$ for the elastic deformation of the tube is:

$$\sigma_{\theta\theta} = \frac{P_1 a^2 - P_2 b^2}{b^2 - a^2} - \frac{a^2 b^2 (P_2 - P_1)}{b^2 - a^2} \frac{1}{r^2}, \tag{2}$$

$$\sigma_{rr} = \frac{P_1 a^2 - P_2 b^2}{b^2 - a^2} + \frac{a^2 b^2 (P_2 - P_1)}{b^2 - a^2} \frac{1}{r^2}, \tag{3}$$

where a is the internal and b is the external radius of the tube.

The Mises plasticity condition in the cylindrical coordinate system is:

$$F = |\sigma_{rr} - \sigma_{\theta\theta}| = 2k, \tag{4}$$

where k is the plastic limit under pure shear conditions, and $k = \sigma_0/\sqrt{3}$, where σ_0 is the plastic limit under pure tension.

Substituting (2) and (3) into (4) we find that if $P_2 > P_1$

$$F = \frac{2a^2 b^2 (P_2 - P_1)}{b^2 - a^2} \frac{1}{r^2}.$$

The function F increases with decreasing r. This means that the plasticity zone will be initiated at the internal surface of the tube if $F = 2k$, or

$$P_2 - P_1 = \frac{k(b^2 - a^2)}{b^2}.$$

As the difference between P_2 and P_1 increases, the plastic zone propagates through the tube towards its outer surface. The whole tube will be in the plastic state if the plastic zone reaches the external radius b.

Substituting (4) into (1) we find that in the plastic zone

$$\frac{d\sigma_{rr}}{dr} = -\frac{2k}{r}. \tag{5}$$

Solving (5) with the boundary condition $\sigma_{rr} = -P_1$ at $r = a$ we find

$$\sigma_{rr} = -2k \ln \frac{r}{a} - P_1. \tag{6}$$

2

The plastic zone reaches $r = b$ if $\sigma_{rr} = -P_2$ at $r = b$. Substituting this condition into (6) we find that this happens if

$$P_2 - P_1 = 2k \ln \frac{b}{a}. \tag{7}$$

Criterion (7) can be used for estimating the confining pressure causing the collapse of a hollow grain.

Given $k = 2 \cdot 10^8$ Pa and $b/a = 1.1$, we find that collapse will occur at the differential pressure $P_2 - P_1 = 380$ bar.

Collapse of a Thin-Walled Shell

Normal stress acting parallel to the surfaces of a thin-walled cylindrical shell under differential pressure P can be easily found as:

$$\sigma = -\frac{PR}{h},$$

where R is the radius and h is the thickness of the shell (see "The Mechanics of Hollow Grains").

Thus the shell collapses if

$$P = \sigma_0 \frac{h}{R} = \sqrt{3} k \frac{h}{R}. \tag{8}$$

Criterion (8) is slightly different from (7). The latter has the following approximate expression as a approaches b:

$$P = 2k \ln(b/a) \approx 2k(b-a)/a = 2kh/a.$$

This difference is due to the thin shells theory approximations.

Conclusions

Assuming that the compaction of pillow basalts and pelagic sediments (both formed by hollow grains) is the result of the collapse of the grains due to increasing confining pressure, we derived simple criteria for the collapse of 2-D thick-walled, and thin-walled circular grains. These criteria can be used for estimating the depth of transition between the low-velocity and the high velocity zones.

Reference

Godfrey, D.E.R., Theoretical Elasticity and Plasticity for Engineers, 1969, Thames and Hudson, London.
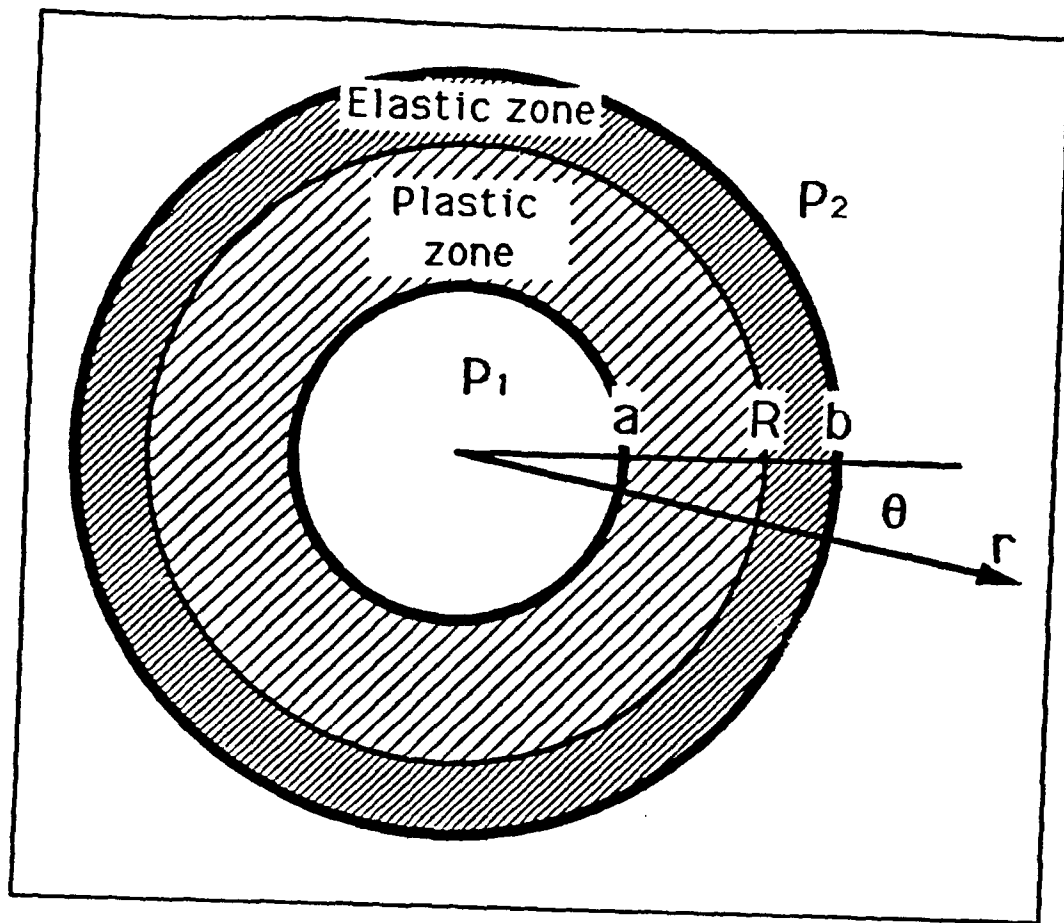
Figure 1 : Elasto-plastic deformation of a thick-walled shell.

Modeling the Seismic Properties of Shallow Oceanic Crust: Effects of Extrusive Morphology on Seismic Velocity

D. Moos, J. Dvorkin, (both at: Dept. of Geophysics, Stanford U., Stanford, CA 94305: 415 723-3464)

Recent seismic data indicate that seismic velocities at the top of very young Oceanic Layer 2 basalts are $V_p \leq 2.5$ km/s and $V_s = 0.6$-0.8 km/s. The low velocity zones (LVZ's) are less than 200 m thick and have velocities that are either independent of depth or increase very slowly. Some results suggest that these zones are absent at ridge crests, increasing in thickness with crustal age. We present here a series of micromechanical models to explain these results in terms of the observed characteristics of the dominant morphologies of extrusive basalts. The principle result of these exercises is that there is no simple relationship between seismic velocities and porosity.

These models rely on the concept of pillow basalts and basalt breccias as granular aggregates of unit elements. The velocity of these aggregates is dependent on the stiffness of the elements and of their contacts. This approach contrasts with effective medium theories, which explain velocity variations by adding to a homogeneous solid material a set of isolated cracks with a well-defined porosity and distribution of aspect ratios. Early results to calculate velocity variations by varying the radius of contact of pillows modeled as solid spherical elements provided a good fit to the velocity data. We present here an extension of the model in which pillow tubes are approximated as thin-walled cylinders. The model can accommodate arbitrary pillow cross sections, and can include radial (cooling) cracks. Depending on wall thickness and the number of cracks, pillow tubes modelled in this way can have very small stiffnesses, resulting in seismic velocities for aggregates composed of these elements that are quite small. An increase in contact pressure accompanying burial has very little effect on the properties of these tubes; however, when the pressure exceeds the strength of the cylinders, they will collapse. At depths corresponding to the collapse pressure, a rapid increase in velocity may result. The results agree qualitatively with seismic data. Coupled with earlier attempts to model contact stiffnesses of pillows, these results extend our efforts to understand the velocity structure of the shallow oceanic crust in terms of the properties of the dominant morphological types.

Anisotropic Poroelasticity and Biot's Parameters

Abstract

Prediction of wave propagation in a submarine environment requires modelling the acoustic response of ocean bottom sediments which generally consists of porous granular materials partially or wholly saturated with water. The effect of anisotropy has to be incorporated into the model in order to simulate more realistic responses.

Following Biot's theory, we present a formulation for seismic wave velocities in a general anisotropic poroelastic medium. We also identify the anisotropic parameters that need to be evaluated or measured for the purpose of estimating the velocities.

Introduction

Poroelasticity or the mechanics of porous media is of fundamental importance in a variety of fields and has received a great deal of attention in recent times. It is believed to play a major role in rock failure phenomena and triggerring of natural and induced seismicity; in proper selection of underground waste disposal sites; enhanced oil recovery; and in underwater acoustics involving wave propagation in water saturated porous marine sediments of the ocean bottom.

Fluid saturation affects the acoustic properties of porous media by tending to stiffen them in compression and to either stiffen or soften them in shear. The effects depend in complicated ways on the geometry and stiffness of the pore space, the stiffness and viscosity of the fluid, the density of all components and the frequency of wave propagation.

The more complex the internal structure and constituents of the rocks, the greater is the number of parameters needed to characterize its properties. For the most simple case of isotropic, elastic, non-porous solid only two

1

independent parameters are needed; four parameters are necessary to characterize an isotropic porous medium while for anisotropic porous media the number increases depending upon the symmetry class of the anisotropy with 28 independent parameters being required for the most general anisotropic poroelastic medium.

Much of our understanding of saturation effects and poroelastic phenomena has been based on the formulations of Biot (1-6) whose equations have formed the basis for solving particular problems in poroelasticity and has long been regarded as a sort of standard. A great deal of the literature pertinent to the study of sediment acoustics (e.g. 7-10) has however focused on the isotropic aspects of Biot's theory and there has been a general lack of using the corresponding anisotropic theory for realistic granular sediments and rocks. We have begun to extend these descriptions to anisotropic porous solids starting with the anisotropic constitutive equations presented by Biot.

Biot's Theory

Biot's theory is a promising approach for modelling acoustic wave propagation in ocean sediments which generally consist of elastic or viscoelastic porous granular materials saturated with water. It is a phenomenological theory with no restrictions being made *a priori* regarding the geometry and shape of cracks and pores. The fluid constituent is modelled as an interconnected compressible continuum within the porous solid matrix, each of them capable of having independent motions. Biot considered both low and high frequency limits in his analysis of propagation of harmonic waves in an unbounded fluid-saturated porous elastic medium and predicted the existence of three kinds of body waves: two compressional or dilational and one rotational. The two distinct types of compressional waves are called the *fast* and *slow* waves or P-waves of the *first* and *second* kind.

The P-waves of the first kind are similar to those observed in ordinary elastic media and is characterized by high phase velocity, small dispersion and low attenuation due to the fact that the motions of the porous frame and the fluid are nearly in phase and hence viscous losses are relatively small. On the other hand, compressional waves of the second kind are diffusive waves, have low phase velocities, large dispersion and are highly attenuated with the frame and fluid components moving largely out of phase. In general it is quite difficult to observe the slow wave in real situations, but the cumulative effect of energy conversion from fast to slow waves at interfaces between dissimilar porous media and between a fluid and a porous medium (e.g.

2

ocean bottom) is quite significant and leads to considerable dissipation of the fast P-wave.

Anisotropic Poroelasticity: Derivations

In this section we present a formulation for estimating seismic velocities in general anisotropic porous solids. Following Biot's theory (5), the constitutive equations for poroelasticity in the most general case of anisotropy may be written as (summation convention implied):

$$\sigma_{ij} = C_{ijkl}e_{kl} + M_{ij}\zeta \tag{1}$$

$$p_f = M_{ij}e_{ij} + M\zeta \tag{2}$$

where σ_{ij} is the stress tensor, e_{kl} is the strain tensor, p_f the fluid pressure, C_{ijkl}, M_{ij} and M are material constants, ζ represents the increment of fluid content and is given by

$$\zeta = -\nabla.\mathbf{w} \tag{3}$$

where

$$\mathbf{w} = \phi(\mathbf{U} - \mathbf{u}) \tag{4}$$

Here $\mathbf{U}$ is the average fluid displacement vector, $\mathbf{u}$ the displacement of the solid matrix and ϕ the porosity.

The equations of motions governing wave propagation are (5): .

$$C_{ijkl}e_{kl,j} + M_{ij}\zeta_{,j} = \rho\ddot{u}_i + \rho_f\ddot{w}_i \tag{5}$$

$$- M_{ij}e_{ij,l} - M\zeta_{,l} = \rho_f\ddot{u}_l + m_{lj}\ddot{w}_j + b_{lj}\dot{w}_j \tag{6}$$

or

$$C_{ijkl}u_{l,kj} - M_{ij}w_{k,kj} = \rho\ddot{u}_i + \rho_f\ddot{w}_i \tag{7}$$

$$- M_{ij}u_{j,il} + Mw_{k,kl} = \rho_f\ddot{u}_l + L_{lj}(w_j) \tag{8}$$

where $\rho = (1 - \phi)\rho_s + \phi\rho_f$, ρ_s and ρ_f being the solid and fluid density respectively. m_{ij} and b_{ij} are the anisotropic virtual mass and drag coefficients, together forming the viscodynamic operator L_{ij}. These six equations for the unknown vector components u_i and w_i govern the propagation of waves in general anisotropic porous media.

First consider the high frequency limit which is the same as the case of an inviscid fluid since for large frequencies the phase velocity with viscous

3

dissipation tends towards that for inviscid fluid. In this limit the term in the first derivative of w_i may be dropped from the second of the two equations of motions. Take plane wave solutions of the form $u_i = A_i f(\tau)$ and $w_i = B_i f(\tau)$ where $\tau = t - n_i x_i / V$, n_i are the components of the unit vector along the direction of propagation and V the phase velocity. Substituting this into equations (7) and (8) after dropping the viscous dissipation term we get:

$$C_{ijkl} n_j n_k A_l - M_{ij} n_k n_j B_k = \rho V^2 A_i + \rho_f V^2 B_i \qquad (9)$$

$$- M_{ij} n_i n_l A_j + M n_k n_l B_k = \rho_f V^2 A_l + m_{lj} V^2 B_j \qquad (10)$$

These formulas can be written as:

$$\Gamma_{il} A_l - \gamma_{ik} B_k = \rho V^2 A_i + \rho_f V^2 B_i \qquad (11)$$

$$- \gamma_{jl} A_j + \theta_{kl} B_k = \rho_f V^2 A_l + m_{lj} V^2 B_j \qquad (12)$$

where $\Gamma_{il} = C_{ijkl} n_j n_k$ is the Christoffel tensor (e.g. 11, 12), $\gamma_{ik} = M_{ij} n_j n_k$ and $\theta_{kl} = M n_k n_l$. Solving equation (12) for **B** gives:

$$\mathbf{B} = (\gamma_{jj} + \rho_f V^2) \mathbf{D}^{-1} \mathbf{A} \qquad (13)$$

with $D_{il} = \theta_{il} - m_{il} V^2$. Substituting this in equation (11) we get

$$\Gamma_{il} A_l - (\gamma_{jj} + \rho_f V^2)^2 (\theta_{il} - m_{il} V^2)^{-1} A_l = \rho V^2 A_i \qquad (14)$$

This can be written in the form of Christoffel's equation as

$$\left(\widetilde{\Gamma_{il}} - \rho V^2 \delta_{il} \right) A_l = 0 \qquad (15)$$

where $\widetilde{\Gamma_{il}}$ is the Poroelastic Christoffel Tensor given by:

$$\widetilde{\Gamma_{il}} = \Gamma_{il} - (\gamma_{jj} + \rho_f V^2)^2 (\theta_{il} - m_{il} V^2)^{-1} \qquad (16)$$

The roots of the determinantal equation

$$\left| \widetilde{\Gamma_{il}} - \rho V^2 \delta_{il} \right| = 0 \qquad (17)$$

give the velocities (or eigenvalues) corresponding to the A_l-eigenvectors. Now if we solve equation (12) for **A** we get

$$A_i = \frac{(\theta_{ik} - m_{ik} V^2)}{(\gamma_{jj} + \rho_f V^2)} B_k \qquad (18)$$

4

which on substituting back in equation (11) gives

$$\left(\tilde{\gamma}_{ik} - \rho_f V^2 \delta_{ik} \right) B_k = 0 \tag{19}$$

where

$$\tilde{\gamma}_{ik} = \frac{(\Gamma_{jj} - \rho V^2)(\theta_{ik} - m_{ik}V^2)}{\gamma_{jj} + \rho_f V^2} - \gamma_{ik} \tag{20}$$

Here again the determinantal equation

$$\left| \tilde{\gamma}_{ik} - \rho_f V^2 \delta_{ik} \right| = 0 \tag{21}$$

gives the eigenvalues corresponding to the B_k-eigenvectors.

Considering two limiting cases: one when $\zeta = -div\mathbf{w} = 0$, the equations of motion reduce to:

$$C_{ijkl}u_{l,kj} = \rho \ddot{u}_i \tag{22}$$

$$M_{ij}u_{j,il} = -\rho_f \ddot{u}_l \tag{23}$$

Again substituting plane wave solutions of the form $u_i = A_i f(t - n_i x_i / V)$ we get:

$$(\Gamma_{il} - \rho V^2 \delta_{il})A_l = 0 \tag{24}$$

$$\gamma_{jl} A_j = -\rho_f V^2 A_l \tag{25}$$

Solving these gives an initial value for V^2 which can be used in equations (16) and (17).

Another limiting case is when $p_f = 0$. Now we get

$$\Gamma_{il} A_l - \gamma_{ik} B_k = \rho V^2 A_i + \rho_f V^2 B_i \tag{26}$$

$$\rho_f A_l + m_{lj} B_j = 0 \tag{27}$$

These two equations ultimately give

$$\left(\widehat{\Gamma_{il}} - \rho V^2 \delta_{il} \right) A_l = 0 \tag{28}$$

with

$$\widehat{\Gamma_{il}} = \Gamma_{il} + \frac{(\gamma_{ii} + \rho_f V^2)\rho_f}{m_{il}} \tag{29}$$

So far the derivation was without fluid viscosity which is appropriate for the high frequency limit. Now taking into account fluid viscosity η

5

and again substituting plane wave solutions in the equations of motions we get a frequency-velocity $(\omega - V)$ relationship expressed in the form of a determinant as:

$$\begin{vmatrix} \rho V^2 \delta_{ij} - \Gamma_{ij} & \rho V^2 \delta_{ij} + \gamma_{ij} \\ \rho_f \omega V^2 \delta_{ij} + \omega \gamma_{ij} & \omega V^2 m_{ij} - i\eta V^2 b_{ij} - \omega \theta_{ij} \end{vmatrix} = 0$$

(30)

Each term is a 3 × 3 determinant making the whole a 6 × 6 one. In the above, the solid skeleton is considered to be perfectly elastic and dissipation is only due to fluid viscosity.

Biot's Parameters

The basic parameters of Biot's theory can be divided into two categories: the passive constants (C_{ijkl}, M_{ij}, M) which depend on the stiffnesses and bulk modulus of the solid and fluid components, their densities and the porosity and a second category (L_{ij} - the viscodynamic operator) which includes a number of interrelated parameters dependent on the relative motion of the fluid with respect to the skeletal frame. The viscodynamic operator involves the first and second derivative with respect to time of the variable w_i.

$$L_{ij} = (m_{ij}\frac{\partial^2}{\partial t^2} + b_{ij}\frac{\partial}{\partial t})$$

(31)

The coefficients m_{ij} and b_{ij} depend on the fabric or microstructure of the constituents and the wave frequency.

The fundamental problems associated with the application of these equations to wave propagation consists of determination of the various moduli and coefficients in terms of the solid, fluid and porous media properties and comparision with suitable experimental data. Perhaps a better understanding of the parameters may be obtained by considering wave propagation in isotropic porous media. Then the equations of motion simplify to (5):

$$\mu u_{i,jj} + (H - \mu)e_{jj,i} - C\zeta_{,i} = \rho \ddot{u}_i + \rho_f \ddot{w}_i$$

(32)

$$Ce_{jj,i} - M\zeta_{,i} = \rho_f \ddot{u}_i + m\ddot{w}_i + b\dot{w}_i$$

(33)

It has been shown (13, 14) that the coefficients H, C, M and μ can be expressed in terms of the porosity, the properties of the fluid and solid

6

constituents and the elastic moduli of the dry porous medium. The results can be written as (15):

$$M = K_s/[1 - K_b/K_s + \phi(K_s/K_f - 1)] \tag{34}$$

$$C = (1 - K_b/K_s)M \tag{35}$$

$$H = (1 - K_b/K_s)C + K_b + (4/3)\mu \tag{36}$$

where K_f is the bulk modulus of the fluid, K_s that of the solid and K_b and μ are the bulk and shear moduli of the dry porous medium, also known as the skeletal frame moduli.

In a few cases these coefficients or some equivalent parameter have been determined for porous material by carrying out jacketed and unjacketed hydrostatic compression tests and shear tests (16, 17, 18). It has been suggested (19), that the moduli of the skeletal frame K_b and μ should be assumed to be complex to account for viscous effects.

Apart from these constitutive constants the equations of motion for a fluid saturated permeable solid also has the frequency dependent viscodynamic operator $L(w_i) = m\ddot{w}_i + b\dot{w}_i$ which contains the inertial drag and viscous dissipative effects due to the pore fluid motion. The simplest form for m and b as originally proposed by Biot is $b = \nu/k$ and $m = \alpha\rho_f/\phi$ where ν is the dynamic fluid viscosity, k the permeability for steady state flow and α is a structure factor for the pore space. This simple form of L is implicitly a low frequency approximation as it uses the steady state Darcy term plus a first order inertial correction term. Biot presented a method for evaluating the drag coefficient by determining the average velocity of liquid in a circular cylinder subject to an oscillating pressure. A closely related method for evaluating the drag and virtual mass coefficients for specific pore geometries has been presented (20) wherein the coefficients are determined by solution of a boundary value problem for a viscous, compressible fluid in a single pore of specified shape. Using finite difference or finite element solutions for fluid displacement it is now feasible to determine (for the isotropic case) the drag and virtual mass coefficients in Biot's equations as a function of frequency for more complicated pore geometries (21).

7

Conclusions

Biot's phenomenological theory for wave propagation in fluid saturated porous media presents a promising framework for modelling the interaction between seismic waves impinging on the sea floor and the submarine sediments. Much work has been done for isotropic porous media. However to simulate more realistic response the effect of anisotropy has to be taken into account.

We have presented a mathematical formulation based on Biot's anisotropic constitutive equations for estimating seismic velocities in a general anisotropic poroelastic medium. Two cases have been considered: that of an inviscid fluid (which is appropriate for the high frequency limit) and that of a viscous fluid, which is valid for all frequencies. In order to solve the determinantal equations for the wave velocities, one needs to know the relevant *anisotropic* rock parameters, the poroelastic material constants and the *anisotropic* virtual mass and drag coefficients which together form the viscodynamic operator.

While measurements and estimates of Biot parameters (both the material constants and the viscodynamic operator) for isotropic material have been made, the corresponding anisotropic Biot coefficients remain to be determined and an important obstacle to the comparision of theory with acoustic measurements in anisotropic porous media still remains.

References

1. Biot, M.A., General theory of three-dimensional consolidation, J.Appl.Phys., **12**, 155-64, 1941.

2. Biot, M.A., Theory of elasticity and consolidation for a porous anisotropic solid, J.Appl.Phys., **26**, 182-185, 1955.

3. Biot, M.A., General solutions of the equations of elasticity and consolidation for a porous material, J.Appl.Mech., **23**, 91-95, 1956.

4. Biot, M.A., Theory of propagation of elastic waves in fluid saturated porous solid - I & II, J.Acoust.Soc.Am., **28**, 168-191, 1956.

5. Biot, M.A., Mechanics of deformation and acoustic propagation in porous media, J.Appl.Phys., **33**, 1482-1498, 1962.

6. Biot, M.A., Generalized theory of acoustic propagation in porous dissipative media, J.Acoust.Soc.Am., **34**, 1256-1264, 1962.

7. Hampton, L.D., Acoustic properties of sediments, J.Acoust.Soc.Am., **42**, 882-890, 1967.

8. Hamilton, E.L., Geoacoustic modelling of the sea floor, J.Acoust. Soc.Am., **68**, 1313-1340, 1980

9. Stoll, R.D., Marine sediment acoustics, J.Acoust.Soc.Am., **77**, 1789-1799, 1985.

9. Stoll, R.D., *Sediment Acoustics*, Springer-Verlag, Berlin, 1989.

10. Auld, B.A., *Acoustic Fields and Waves in Solids*, v. I & II, John Wiley & Sons., New York, 1973.

11. Beltzer, A.I., *Acoustics of solids*, Springer-Verlag, Berlin, 1988.

12. Biot, M.A.& Willis, D.G., The elastic coefficients of the theory of consolidation, J.Appl.Mech., **24**, 594-601, 1957.

13. Geertsma, J.& Smit, D.C., Some aspects of elastic wave propagation in fluid saturated porous soilds, Geophysics, **26**, 169-181, 1961.

14. Bedford, A.,Stern, M.& Costley, R.D., On the application of Biot's equation to saturated marine sediments, *in* Multiple scattering of waves in random media and random rough surfaces., 329-340, The Pennsylvania State University, 1985.

15. Fatt, I.,The Biot-Willis elastic coefficients for a sandstone, J.Appl.Mech., **26**, 296-297, 1959.

16. Yew, C.H.& Jogi, P.N., The determination of Biot's parameters for sandstones, part I : static tests, Exptl.Mech. **18**, 167-178, 1978.

17. Green, D.H.& Wang, H.F., Fluid pressure response to undrained compression in saturated sedimentary rock, Geophysics, **51**, 948-956, 1986.

18. Stoll, R.D.& Bryan, G.M., Wave attenuation in saturated sediments, J.Acoust.Soc.Am., **47**, 1440-1447, 1969.

19. Bedford, A.,Costley, R.D.& Stern, M., On the drag and virtual mass coefficients in Biot's equations, J.Acoust.Soc.Am., **76**, 1804-1809, 1984.

20. Yavari, B.& Bedford, A., Computation of the Biot drag and virtual mass coefficients, Int.J.Multiphase Flow, **14**, 1-12, 1988.

9